MOLECULAR PHYSICS, 10–20 DECEMBER 2003, VOL. 101, NOS. 23–24, 3349–3384

Taylor & Francis
Taylor & Francis Group

Invited article

Statistical mechanics of inhomogeneous model colloid–polymer mixtures

JOSEPH M. BRADER[1], ROBERT EVANS[2,3]*† and MATTHIAS SCHMIDT[4]‡

[1]Institute of Physiology, University of Bern, Bühlplatz 5, 3012 Bern, Switzerland
[2]H. H. Wills Physics Laboratory, University of Bristol, Royal Fort, Tyndall Avenue, Bristol BS8 1TL, UK
[3]MPI für Metallforschung, Heisenbergstraße 3, D-70569 Stuttgart, Germany
[4]Soft Condensed Matter, Debye Institut, Utrecht University, Princetonplein 5, 3584 CC Utrecht, The Netherlands

(*Received 22 September 2003; revised version accepted 10 November 2003*)

We describe two strategies for tackling the equilibrium statistical mechanics of inhomogeneous colloid–polymer mixtures treated in terms of the simple Asakura–Oosawa–Vrij (AO) model, in which colloid–colloid and colloid–polymer interactions are hard-sphere like, whereas the polymer–polymer interaction is zero (perfectly interpenetrating polymer spheres). The first strategy is based upon integrating out the degrees of freedom of the polymer spheres to obtain an effective one-component Hamiltonian for the colloids. This is particularly effective for small size ratios $q = \sigma_p/\sigma_c < 0.1547$, where σ_p and σ_c are the diameters of colloid and polymer spheres, respectively, since in this regime three and higher body contributions to the effective Hamiltonian vanish. In the second strategy we employ a geometry based density functional theory (DFT), specifically designed for the AO model but based on Rosenfeld's fundamental measure DFT for additive mixtures of hard-spheres, that treats colloid and polymer on an equal footing and which accounts for the fluid–fluid phase separation occurring for larger values of q. Using the DFT we investigate the properties of the 'free' interface between colloid-rich (liquid) and colloid-poor (gas) fluid phases and adsorption phenomena at the interface between the AO mixture and a hard-wall, for a wide range of size ratios. In particular, for $q = 0.6$ to 1.0, we find rich interfacial phenomena, including oscillatory density profiles at the free interface and novel wetting and layering phase transitions at the hard-wall–colloid gas interface. Where appropriate we compare our DFT results with those from computer simulations and experiment. We outline several very recent extensions of the basic AO model for which geometry based DFTs have also been developed. These include a model in which the effective polymer sphere–polymer sphere interaction is treated as a repulsive step function rather than ideal and one in which the depletant is a fluid of infinitely thin rods (needles) with orientational degrees of freedom rather than (non-interacting) polymer spheres. We comment on the differences between results obtained from these extensions and those of the basic AO model. Whilst the interfacial properties of the AO model share features in common with the those of simple (atomic) fluids, with the polymer reservoir density replacing the inverse temperature, we emphasize that there are important differences which are related to the many-body character of the effective one-component Hamiltonian.

1. Introduction

It is well established that certain colloidal suspensions behave as hard-sphere systems. Pioneering studies by Pusey, van Megen and co-workers in the 1980s established that polymethylmethacrylate (PMMA) particles, sterically stabilized by chemically grafted poly-12-hydroxystearic acid (PHSA), dispersed in a solvent whose refractive index matches that of the particles, exhibit phase behaviour which mimics closely that of pure hard spheres [1]. In particular, coexistence of colloidal fluid and crystal phases was found for colloid packing (volume) fractions, η_c, in the range $0.494 < \eta_c < 0.545$, values consistent with computer simulations

*Author for correspondence. e-mail: bob.evans@bristol.ac.uk

†Molecular Physics Lecture, Liblice Conference, Czech Republic, June 2002. Invited paper for journal.

‡On leave from Institut für Theoretische Physik II, Heinrich-Heine-Universität Düsseldorf, Universitätsstraße 1, D-40225 Düsseldorf, Germany.

Molecular Physics ISSN 0026–8976 print/ISSN 1362–3028 online © 2003 Taylor & Francis Ltd
http://www.tandf.co.uk/journals
DOI: 10.1080/0026897032000174263

of hard spheres. For $\eta_c < 0.494$ there is a single fluid phase in which the diffusive dynamics of the colloidal particles, as measured by dynamic light scattering, is consistent with hard-sphere behaviour [1]. Other colloidal systems also behave as hard spheres. For example, the equation of state, obtained from X-ray measurements of the colloid density profile in a gravitational field, for charged polystyrene spheres suspended in water (with HCl) is in excellent agreement with the hard-sphere equation of state, on both the fluid and crystal branches [2]. Of course, the effective pair potential between colloids cannot be perfectly hard; this cannot jump discontinuously to infinite repulsion at some precise diameter. However, as the particles approach each other the effective potential rises by many k_BT over a separation of one or two nanometres or so—a distance which is very small compared with the particle diameter (typically 6–700 nm, in the experiments mentioned above). Entropically driven freezing is the *only* phase transition that can occur in a system of 'hard-sphere' colloids.

Suppose now that non-adsorbing polymer is added to the suspension of colloids. The interactions are, in general, complicated but one can consider the case of flexible polymer chains under athermal 'good'-solvent conditions, where the interactions between all the species are hard-core repulsive, i.e. polymer chains are mutually self-avoiding and are excluded from the hard-sphere colloids. From a statistical mechanics point of view, only packing constraints are relevant and the properties of the system, in particular any phase transitions, are determined by purely entropic effects. It then comes as something of a surprise to learn that the phase behaviour of colloid–polymer mixtures can be very rich. A series of experiments, performed mainly by groups in Utrecht, Bristol and Edinburgh in the 1980s and early 1990s, confirmed that adding sufficient non-adsorbing polymers can cause phase separation into two fluid phases, one rich in colloid and the other poor; references to the original papers can be found in [1, 3–5]. In order for fluid–fluid phase separation to occur there must be a mechanism that generates an effective attractive interaction between the colloidal particles. Moreover, this mechanism must be entropic in origin since all 'bare' interactions between species are hard-core repulsive. An appropriate mechanism was described as early as 1954 by Asakura and Oosawa [6] and this is now termed the depletion effect or depletion attraction. Asakura and Oosawa considered two big spherical colloidal particles in a 'sea' of rigid macromolecules. The latter were treated as hard spheres as regards their interaction with the colloids whereas macromolecule–macromolecule were set to zero, so that the solution of macromolecules was treated as an ideal gas. Such an assumption should be appropriate for a dilute solution or for theta solvents where the second virial coefficient for macromolecule–macromolecule interactions vanishes. The centre of a macromolecule sphere is excluded from the surface of a colloid by a distance equal to $\sigma_p/2$, so there is a depletion zone (or excluded volume region) in which there are no macromolecule centres of mass. If two colloids approach each other, so that the depletion zones overlap, then there is an increase in free volume for the macromolecule spheres, i.e. an increase in their translational entropy, leading to an effective attractive (depletion) interaction between the two colloids. One can also view the attraction as arising from an unbalanced osmotic pressure pushing the colloids together as the macromolecules are expelled from the gap between the two colloids. By calculating the volume of the overlap between the two depletion zones, Asakura and Oosawa [6] obtained an explicit expression for the depletion force between two colloids whose centres are separated by a distance R, immersed in an ideal solution of macromolecules of fugacity z_p. The depletion potential $\phi_{AO}(R; z_p)$ vanishes when the depletion zones no longer overlap; the attractive potential has a finite range equal to σ_p. Increasing the concentration of the macromolecule sea increases z_p and the depth of the potential well, whereas increasing σ_p extends the range and, hence, the integrated strength of the attraction. It is clear that depletion attraction is a possible mechanism for driving phase separation. In a second paper, Asakura and Oosawa [7] focused on the depletion potential and discussed the possible aggregation of suspended colloidal particles. By assuming the polymers can be treated as spherical macromolecules, internal conformational degrees of freedom are ignored. Independently, in 1976 Vrij [8] proposed the same depletion mechanism, deduced the depletion potential between a pair of colloidal spheres and the associated second virial coefficient and went an important step further by writing down an explicit model Hamiltonian for the binary *mixture* of hard-sphere colloids and ideal polymer (macromolecule) spheres; this is the Asakura–Oosawa–Vrij or AO model—see section 2. Vrij's paper provides the basis for a full statistical mechanical treatment for an (idealized) model of a colloid–polymer mixture. Vrij pointed out that his interparticle potentials define a 'non-additive' hard-sphere model in the the theory of liquids. We return to this aspect in section 2. He also suggested that the colloid–polymer hard-sphere diameter should be $(\sigma_c + \sigma_p)/2$ with $\sigma_p/2 \sim R_g$, the radius of gyration of the polymer. The next important development in the theory was made by Gast *et al.* [9] who calculated the phase behaviour of the AO model using thermodynamic perturbation theories for an

approximation that assumes an effective colloid–colloid pair potential, $\phi^{\text{eff}}(R; z_p)$, consisting of the bare hard-sphere potential plus the attractive depletion potential $\phi_{AO}(R; z_p)$. Gast *et al*. predicted that the effect of adding polymer depends sensitively on the polymer to colloid size ratio $q = \sigma_p/\sigma_c$. For $q \lesssim 0.3$, adding polymer merely augments, in η_c, the colloidal fluid–crystal coexistence region above the range found for pure hard spheres, whereas for larger values of q a stable colloidal *liquid* phase can exist. In the (η_c, z_p) plane there is a triple point where gas, liquid and crystalline colloidal phases coexist [9] and for $q \gtrsim 0.6$ the phase diagrams resemble those of simple atomic fluids, with z_p playing the same role as inverse temperature, $1/T$. Thus, entropically driven depletion attraction can become sufficiently strong and sufficiently long-ranged to generate a van der Waals-like scenario for the gas-liquid transition.

As noted by Gast *et al*., one significant drawback to their approach is that for size ratios $q > 0.1547$, the effective one-component Hamiltonian should contain three- and higher-body effective interactions between the colloidal particles—see section 2.1; these interactions are tedious to evaluate and cumbersome to incorporate into perturbation theories or computer simulations of the liquid and crystalline phases and are therefore usually ignored. However, the effects of many-body effective interactions are not necessarily small and we shall argue below that these can play a crucial role for both bulk and interfacial phase behaviour.

An alternative approach to determining the phase behaviour of the AO model, which does not rely upon mapping to an effective one-component Hamiltonian and which *does* capture some of the effects of many-body terms, is the so-called free-volume theory of Lekkerkerker *et al*. [4]. Some details of this approach will be given in section 2.2 but the approximation consists of replacing the exact (average) free volume available to the ideal polymers by the corresponding quantity evaluated in the low-density limit, $z_p \to 0$, for which an analytical approximation is available. Having an explicit expression for the free volume fraction, $\alpha(\eta_c)$, allows one to transform readily from the reservoir representation, where z_p or, equivalently, η_p^r, the packing fraction of ideal polymer is specified, to the system representation where η_p, the packing fraction in the actual system is specified: $\eta_p = \alpha\eta_p^r$. Experimental phase diagrams are plotted in the (η_c, η_p) plane. The free-volume theory predicts a stable colloidal gas–liquid transition for $q \gtrsim 0.32$ and the phase diagrams exhibit similar trends to those from the approach of Gast *et al*., although there are some significant differences—see [10] for detailed comparisons and [11] for a discussion of the connections and distinctions between the two approaches. Subsequently Meijer and Frenkel [3] performed pioneering Monte Carlo simulations for two separate models of colloids dispersed in a dilute polymer solution. The first was a lattice–polymer model in which polymers are represented by *ideal* (non-self-avoiding) chains confined to a cubic lattice. However, lattice sites occupied by colloidal hard-spheres are inaccessible to polymer. The second was the AO model, but with the polymer spheres restricted to a cubic lattice. Phase diagrams, calculated in the (η_c, z_p) plane, for the two models were rather close to each other and for the size ratios $q = 0.5$ and 0.7 considered the simulation results corresponding to the (lattice–polymer) AO model were in fair agreement with those from free-volume theory.

To summarize, by 1994 various theoretical and simulation studies of idealized models had shown that for small polymer–colloid size ratios the phase diagram is of the fluid–solid type, whereas for larger size ratios, where the depletion potential becomes longer ranged *and* many-body interactions become important, stable colloidal gas–liquid phase separation occurs. This trend in the phase behaviour was consistent with earlier experimental observations. Subsequent experiments [5, 12] provided convincing support for the scenario suggested by theory. In particular, three-phase coexistence was reported at certain size ratios for charged colloidal polystyrene particles mixed with hydroxyethyl cellulose [12] and for sterically stabilized PMMA particles mixed with random coil polystyrene (PS) in a *cis*-decalin solvent [5]. An admirable account of the work of the Edinburgh group on the latter system, which the author describes as a 'model colloid–polymer mixture', is given in the recent topical review by Poon [13]. We direct readers wishing to learn more about phase behaviour, equilibrium structure, phase transition kinetics, gels and glasses in *real* mixtures to this illuminating article. Another well-characterized system, much studied by the Utrecht group, consists of sterically stabilized silica particles and polydimethylsiloxane (PDMS) in cyclohexane. Silica has the advantage over PMMA that small particles are available (diameters as small as 20 nm) which is important in studies of interfaces—see section 3.

The thrust of the present article is quite different from that of Poon. Having established that the simple AO model captures the main features of the experimental bulk phase diagrams, here we enquire what are the properties of *inhomogeneous* colloid–polymer mixtures, as described by the same AO model. Inhomogeneous situations, where the average density profiles of both species are spatially varying, occur in the context of adsorption at a solid substrate, at the planar interface between two coexisting (colloid-rich and colloid-poor) phases, for mixtures confined in capillaries or porous

media or, indeed, in a colloidal crystal. Nucleation phenomena also require a description of the inhomogeneous fluid. Our strategy is not to attempt any realistic modelling of a colloid–polymer mixture which is, of course, a highly complex system involving multiple length and time scales, rather we seek to understand the basic adsorption and interfacial properties that arise in the context of the simple model fluids. Moreover, we restrict consideration to equilibrium aspects. Whether the predictions from the model are relevant to real mixtures is a separate issue. In defence of our strategy we remark (as humble theorists!) that without detailed theoretical and simulation studies of the Lennard-Jones and other model fluids, we would have little fundamental understanding of the properties of simple, atomic liquids at interfaces or under confinement—the experimentalists are certainly catching up but experiments on fluid interfaces are notoriously difficult. One might go further and argue that studies of the Ising or lattice gas model, with the substrate treated as an external field, led to a wealth of predictions for surface phase transitions most of which were found in adsorption experiments. Let us be clear, however. We are not suggesting that the AO model has the same significance in statistical physics as the Ising model! Nevertheless, the AO model has much appeal to the theorist. There is only one parameter, the size ratio q, and by varying q different types of bulk phase behaviour emerge. Moreover, we find that the same model predicts striking interfacial phenomena, some of which are very different from those found for simple fluids and which reflect the special character of the effective interactions in the AO model.

Those readers who are interested in recent developments in the theory of more realistic models of colloid–polymer mixtures are referred to the topical review by Fuchs and Schweizer [14] who describe liquid-state integral equation theories for tackling structural correlations starting at the polymer segment level. The polymers are treated as connected chains of segments which experience excluded-volume forces among themselves and with the hard-sphere colloids. Although the integral equation approaches provide much insight into the nature of correlations for a wide range of size ratios (including $q \gg 1$) and for a variety of polymer concentrations, they appear to be restricted to homogeneous (bulk) fluids and it is difficult to envisage extensions to inhomogeneous systems or to crystalline phases, i.e. to the full phase diagram. Very recently, Bolhuis and co-workers [15] have performed Monte Carlo simulations of the bulk phase diagram of a model in which the colloids are treated as hard spheres and the polymers as self-avoiding walks that are mapped to an effective pair potential. We shall make reference to their work in section 5.2, but for more details of this powerful 'polymers as soft colloids' computational approach readers should consult the original paper and references therein.

The present article is organized as follows. In section 2 we describe the AO model Hamiltonian and two different strategies for tackling its statistical mechanics. The first is to integrate out the degrees of freedom of the polymer spheres, thereby obtaining an effective one-component Hamiltonian for the colloidal hard spheres. As mentioned above, this approach is particularly effective for small size ratios, $q < 0.1547$, where the one-component Hamiltonian consists of zero, one and two-body contributions only; there are no higher-body effective interactions. The second strategy is to tackle the binary AO mixture directly; the two components are treated on equal footing by means of a geometry-based density functional theory that is specifically designed for the inhomogeneous AO mixture [16, 17]. The procedure for constructing the DFT is based on the fundamental measure theory developed by Rosenfeld [18] for additive hard-sphere mixtures. For uniform (bulk) fluids the free energy obtained from the DFT is identical to that given by the free-volume theory of Lekkerkerker *et al.* [4] alluded to above. Section 3 describes an application of the DFT to the planar interface between demixed fluid phases, one rich in colloid, the other poor. We find that for coexisting states well away from the critical point, at high polymer fugacity, both the colloid and polymer density profiles exhibit oscillations on the colloid-rich (liquid) side of the interface. We also discuss the behaviour of the surface tension comparing with experimental results. In section 4 we consider adsorption of the AO mixture at a planar hard wall. When a colloidal particle is sufficiently close to a hard wall, such that the two depletion zones overlap, there is an effective attractive potential between the two which is similar to the potential, ϕ_{AO}, between two colloidal particles, i.e. expulsion of polymer induces an attractive wall–colloid depletion potential $\phi_{\mathrm{AO}}^{\mathrm{wall}}$ whose range is equal to σ_{p}. For small size ratios q, very large contact densities are found for the colloid profile $\rho_{\mathrm{c}}(z)$, reflecting the form of $\phi_{\mathrm{AO}}^{\mathrm{wall}}(z; z_{\mathrm{p}})$. For larger q fluid–fluid phase separation can occur and we find novel entropic wetting and layering transitions using the DFT—see section 4.2. Results of recent computer simulations of the AO mixture, with $q = 1$, adsorbed at a hard wall are described in section 4.3; these also predict wetting and layering transitions [19]. Section 5 describes a recent extension of the DFT approach that incorporates, albeit in a simple way, polymer–polymer interactions [20]. In the 'soft colloid' picture [21] of polymers, segment–segment repulsion, averaged over conformations of the chains, leads to an effective

interaction, ϕ_{pp}, between the polymer centres of mass that is repulsive, soft and penetrable. By making the crude approximation that $\phi_{pp}(r)$ is a step-function pair potential of height ϵ, it is possible to construct a geometry-based DFT for a model that has as its limiting cases: (i) the AO model ($\epsilon = 0$, non-interacting polymer) and (ii) the binary hard-sphere mixture ($\epsilon \to \infty$). We present results for fluid–fluid phase separation, comparing with those for the AO model and with computer simulations. In section 6 we summarize briefly some other recent applications and extensions of the DFT for the AO model. Several of these are concerned with bulk properties only but we also describe recent work on mixtures of hard-sphere colloids and hard needles, modelling experimentally realizable stiff colloidal rods, where interfacial properties were considered [22–24]. This model system shares many features in common with the AO model—the needles act as the depletant. It has the additional feature of orientational degrees of freedom for the needles which can introduce orientational ordering at an interface, even though the bulk fluid is isotropic (the infinitely thin rods cannot interact). We conclude in section 7 with some remarks and an outlook on future work.

What follows is not intended to be a review of what is a large and rapidly developing literature on the experimental, theoretical and simulation aspects of colloid–polymer mixtures; we make no attempt to give a comprehensive overview or an exhaustive list of references. For example, we concentrate on the so-called 'colloid limit', $q \lesssim 1$, rather than the equally important 'protein or nanoparticle limit', $q \gg 1$, where the physics is, arguably, less understood. The choice of material reflects the personal viewpoints of the authors on the subject area and the presentation is based, in part, on the Molecular Physics Lecture given by R. Evans at the Liblice Conference in June 2002. Although much of the theoretical background has been published elsewhere, almost all the results presented in sections 3 and 4 appear for the first time: they are from the unpublished thesis of Brader [25]. Section 5.2 also contains new results. A brief summary of some of the earlier work can be found in a conference article [26].

2. The Asakura–Oosawa–Vrij model

We consider a suspension of sterically stabilized colloidal particles immersed together with non-adsorbing polymers in an organic solvent. The interaction between two sterically stabilized colloidal particles in an organic solvent is close to that between hard spheres, whereas dilute solutions of polymers in a theta-solvent can be represented by non-interacting or ideal polymers. A simple idealized model for such a colloid–polymer mixture is the so-called Asakura–Oosawa–Vrij (AO) model [6–8]. This is an extreme non-additive binary hard-sphere model in which the colloids are treated as hard spheres with diameter σ_c and the interpenetrable, non-interacting polymer coils are treated as point particles but which are excluded from the colloids to a centre-of-mass distance of $(\sigma_c + \sigma_p)/2$. The diameter of the polymer sphere is $\sigma_p = 2R_g$ with R_g the radius of gyration of the polymer. The pairwise potentials in this simple model are given by

$$\phi_{cc}(R_{ij}) = \begin{cases} \infty, & \text{for } R_{ij} < \sigma_c, \\ 0, & \text{otherwise}, \end{cases}$$
$$\phi_{cp}(|\mathbf{R}_i - \mathbf{r}_j|) = \begin{cases} \infty, & \text{for } |\mathbf{R}_i - \mathbf{r}_j| < \tfrac{1}{2}(\sigma_c + \sigma_p), \\ 0, & \text{otherwise}, \end{cases}$$
$$\phi_{pp}(r_{ij}) = 0, \tag{1}$$

where $\mathbf{R}$ and $\mathbf{r}$ denote colloid and polymer centre-of-mass coordinates, respectively, with $R_{ij} = |\mathbf{R}_i - \mathbf{R}_j|$ and $r_{ij} = |\mathbf{r}_i - \mathbf{r}_j|$. Note that a general non-additive binary hard-sphere mixture is described by the 'diameters' σ_{11}, σ_{22} and σ_{12}, where subscripts 1 and 2 denote species 1 and 2. The cross-term is given by $\sigma_{12} = (\sigma_{11} + \sigma_{22}) \times (1 + \Delta)/2$, where the non-additivity parameter Δ is zero for additive mixtures. The AO model corresponds to $\sigma_{22} = 0$ and $\Delta = q$, the fixed size ratio σ_p/σ_c. The Hamiltonian of the AO model consists of (trivial) kinetic contributions and a sum of interaction terms: $H = H_{cc} + H_{cp} + H_{pp}$, where

$$H_{cc} = \sum_{i<j}^{N_c} \phi_{cc}(R_{ij}),$$
$$H_{cp} = \sum_{i}^{N_c} \sum_{j}^{N_p} \phi_{cp}(|\mathbf{R}_i - \mathbf{r}_j|),$$
$$H_{pp} = \sum_{i<j}^{N_p} \phi_{pp}(R_{ij}) = 0 \tag{2}$$

and we consider N_c colloids and N_p ideal polymers in a volume V at temperature T. The solvent is regarded as an inert continuum. See figure 1 (*a*) for an illustration of the model.

There are several ways of tackling the statistical mechanics of the AO model. Brute force, direct computer simulations of this model mixture are not straightforward since problems of slow equilibration and non-ergodicity can arise for large size asymmetries, where huge numbers of polymers are required per colloid particle. Recently, however, simulation studies have been carried out for several values of the size ratio $q = \sigma_p/\sigma_c$

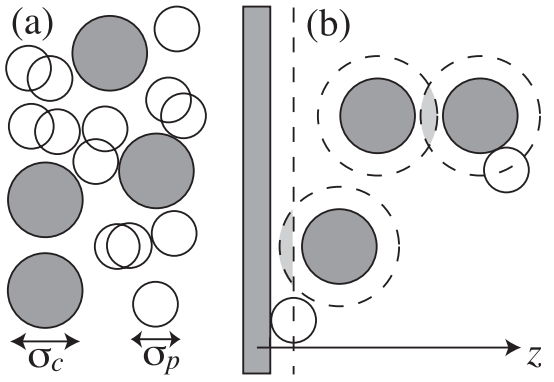

Figure 1. (*a*) Sketch of the Asakura–Oosawa–Vrij model of hard spheres (grey circles) with diameter σ_c and ideal polymers (white circles) with diameter σ_p. (*b*) Depletion zones (dashed lines) that are inaccessible to polymer centres. Overlapping depletion zones (light grey shapes) are indicated in two cases, that between two colloids and that between a colloid and a hard wall.

and we shall report on these in section 4.3. Here we describe two alternative approaches which have been successfully employed. The first is most appropriate for mixtures where the size ratio $q \ll 1$; it depends upon integrating out the degrees of freedom of the ideal polymer to obtain an effective one-component Hamiltonian for the colloids. The second approach employs a density-functional theory designed specifically for the AO mixture; this treats both species on an equal footing.

2.1. *The effective one-component Hamiltonian*

For a general binary mixture it is possible to construct an effective one-component Hamiltonian for one of the components—usually the larger species—by integrating out the degrees of freedom of the other—usually the smaller species [27]. As usual it is convenient to work in the semi-grand ensemble where (N_c, z_p, V, T) are fixed variables, i.e. the fugacity $z_p = \Lambda_p^{-3} \exp(\beta\mu_p)$ of a reservoir of polymer is fixed. μ_p is the chemical potential, $\beta = 1/k_B T$ and Λ_p is the thermal de Broglie wavelength of the polymer. In order to treat inhomogeneous fluids it is also convenient to allow the colloids and polymer to couple independently to two external fields. Thus one adds to the Hamiltonian H contributions

$$V_c^{ext} = \sum_{i=1}^{N_c} V_c^{ext}(\mathbf{R}_i), \qquad V_p^{ext} = \sum_{i=1}^{N_p} V_p^{ext}(\mathbf{r}_i), \tag{3}$$

which can produce inhomogeneous density profiles. It is straightforward to show that the semi-grand free energy $F(N_c, V, z_p)$ is given by

$$\exp(-\beta F) = \frac{1}{N_c! \Lambda_c^{3N_c}} \int d\mathbf{R}^{N_c} \exp\left(-\beta(H_{cc} + \Omega + V_c^{ext})\right), \tag{4}$$

where Λ_c is the thermal de Broglie wavelength of the colloid and

$$\exp(-\beta\Omega) = \sum_{N_p=0}^{\infty} \frac{z_p^{N_p}}{N_p!} \int d\mathbf{r}^{N_p} \exp\left(-\beta(H_{cp} + V_p^{ext})\right). \tag{5}$$

Ω is simply the grand potential of the (ideal) polymer in the presence of the external field arising from (a) a fixed configuration $\{\mathbf{R}^{N_c}\}$ of N_c colloids and (b) any applied field V_p^{ext}. Provided one can determine Ω explicitly, or at least a good approximation to Ω, the binary mixture problem is reduced to a simpler one-component problem: equation (4) describes a system of colloids interacting through an effective Hamiltonian: $H^{eff} = H_{cc} + \Omega + V_c^{ext}$.

In a general mixture Ω consists of zero, one, two, ..., many-body contributions [28] and the resulting H^{eff} is unwieldy. However, for the particular case of the AO model the contributions simplify [10, 11] because the polymer is ideal, i.e. $\phi_{pp} = 0$. Moreover, for a homogeneous fluid, with no external potentials, the series truncates after the two-body term, provided that $q < 2/3^{1/2} - 1 = 0.1547$ [9, 10]. For such high asymmetry there is no triple overlap of excluded volume regions, even when three colloids are in simultaneous contact. Thus, for $q < 0.1547$, geometrical considerations ensure that there is an *exact* mapping from the bulk binary mixture to an effective Hamiltonian that contains only two-body interactions plus structure (configuration) independent contributions. The effective pair potential is given by [9, 10]

$$\phi^{eff}(R; z_p) = \phi_{cc}(R) + \phi_{AO}(R; z_p), \tag{6}$$

where $\phi_{AO}(R; z_p)$ is the well-known AO pair (depletion) potential between two hard-sphere colloids in a sea of ideal polymer [6, 7], see figure 1 (*b*) for an illustration. $\phi_{AO}(R; z_p)$ is attractive and has a finite range equal to σ_p. Its strength is proportional to z_p and it can be expressed as a polynomial in $s = R/\sigma_c$:

$$\beta\phi_{AO}(R; z_p) = \begin{cases} -\frac{\pi}{6}\sigma_p^3 z_p (1+q^{-1})^3 \left[1 - \frac{3s}{2(1+q)} + \frac{s^3}{2(1+q)^3}\right], & \\ \qquad 1 < s < 1+q, & \\ 0, \qquad s > 1+q. & \end{cases} \tag{7}$$

Perhaps more remarkably, Brader *et al.* [11] showed that for the AO mixture in contact with a hard wall defined by the external potentials

$$V_c^{ext}(z) = \begin{cases} \infty, & z < \sigma_c/2, \\ 0, & z \geq \sigma_c/2, \end{cases}$$
$$V_p^{ext}(z) = \begin{cases} \infty, & z < \sigma_p/2, \\ 0 & z \geq \sigma_p/2, \end{cases} \quad (8)$$

where z is the centre of the particle measured normal to the wall, there is also an exact mapping of the binary mixture to a simple effective Hamiltonian. Using geometrical considerations (see figure 2 of [11]) they showed that for $q < 0.25$ all many-body terms Ω_n, with $n \geq 2$, are unaltered from their form in the bulk (homogeneous) fluid by the presence of the hard wall. For larger values of q the two-body potential becomes a complicated function of $\mathbf{R}_1$ and $\mathbf{R}_2$ and is not simply a function of the separation $|\mathbf{R}_1 - \mathbf{R}_2|$. Specifically, for $q < 0.1547$, the effective Hamiltonian for the inhomogeneous fluid at the hard wall reduces to

$$H^{eff} = H_{cc} + \sum_{i=1}^{N_c} V_c^{ext}(z_i) + \sum_{i=1}^{N_c} \phi_{AO}^{wall}(z_i; z_p) + \Omega_0^{bulk} + \Omega_1^{bulk} + \sum_{i<j} \phi_{AO}(R_{ij}; z_p). \quad (9)$$

The additional one-body term ϕ_{AO}^{wall} represents the attractive AO depletion potential between the colloid and the planar hard wall. This potential has the same range, σ_p, as ϕ_{AO} and it has similar form [11]. In the absence of the wall equation (9) reduces to the effective Hamiltonian of the homogeneous system. The structure-independent terms are given by

$$-\beta\Omega_0^{bulk} = z_p V,$$
$$-\beta\Omega_1^{bulk} = -z_p N_c \pi (\sigma_c + \sigma_p)^3/6 = -z_p \eta_c (1+q)^3 V, \quad (10)$$

where $\eta_c = (\pi/6)\sigma_c^3 N_c/V$ is the colloid packing fraction.

Having such a simple effective Hamiltonian for the homogeneous fluid means that it is straightforward to perform computer simulations or to implement standard one-component integral equation closures. Recall that integral equation approaches for highly asymmetric *mixtures* are especially problematical whereas Percus–Yevick (PY) and similar closures provide a reliable description of the pair correlation function for a one-component fluid whose pair potential consists of a hard core plus an attractive tail. Of course, the usual issues of thermodynamic inconsistency remain.

Dijkstra *et al.* [10] carried out extensive investigations of the properties of the bulk mixture with $q = 0.1$ using the effective Hamiltonian. The equilibrium structure, i.e. the colloid–colloid radial distribution function $g_{cc}(R)$ and the structure factor $S_{cc}(k)$, is determined solely by $\phi^{eff}(R; z_p)$, equation (6), for this size ratio and Monte Carlo and PY results at various colloid packing fractions are presented in [10]. Note that since the terms Ω_0^{bulk} and Ω_1^{bulk} depend linearly on N_c or V they have no effect on bulk phase equilibria and the latter is, once again, determined solely by the pair potential $\phi^{eff}(R; z_p)$ [10, 28]. (These terms do contribute to the total pressure and total compressibility of the mixture, however [29].) The complete equilibrium phase diagram of the mixture was determined by simulation of the effective one-component system for $q = 0.1$. It is extremely rich, displaying a very broad, in η_c, fluid–solid coexistence curve which lies at lower polymer densities than a (metastable) fluid–fluid coexistence region. There is also an isostructural (fcc) solid–solid transition which is very slightly metastable with respect to the fluid–solid transition [10, 11]. Note that as each term in the effective Hamiltonian is proportional to z_p ($\equiv$ polymer density in the reservoir, ρ_p^r, for ideal polymer) this variable plays the same role as inverse temperature in simple atomic fluids. Thus, phase diagrams plotted in the (η_c, z_p) plane often display features similar to those plotted in the (density, $1/T$) plane for simple fluids. The simulation results for the bulk system provide a valuable benchmark against which approximate theories, e.g. integral equation, density functional or perturbation theory approaches, can be tested [10].

Similar remarks apply to the Monte Carlo simulation results obtained using the effective Hamiltonian (9) for the mixture at a planar hard wall. Brader *et al.* [11] considered the AO mixture, with $q = 0.1$, for two fixed values of the colloid packing fraction, $\eta_c = 0.3$ and 0.4, and increasing amounts of polymer. Adding polymer (increasing z_p) leads to increased depletion attraction for the colloids at the hard wall which leads, in turn, to pronounced effects on the density profile near the wall. We shall comment further on this phenomenon in section 4.1 where we compare results from density functional theory with those of the simulations.

We conclude this subsection by making some remarks about the form of the effective Hamiltonian to be used for other types of inhomogeneity. If the wall–fluid potentials are soft or exhibit attractive portions then the integrating out of the polymer can lead to more complex contributions, even for small size ratios q. On the other hand, for *spontaneously* generated inhomogeneities, where the density profiles of colloid and of polymer are spatially varying in vanishing external fields, the appropriate effective Hamiltonian is that of the bulk, homogeneous system [11]. Relevant examples

are the planar interface between demixed fluid phases, colloidal crystals where the densities vary periodically, and the fluid–crystal interface. Although the distribution of polymer in a colloidal crystal or in the region of any interface is very different from that in a bulk fluid this does *not* give rise to different effective interactions, in the sense that the effective Hamiltonian needs to be modified. Since we work in the semi-grand ensemble, with a reservoir of polymer, it is solely the fugacity z_p that determines all the effective interactions in the system. As z_p is constant throughout the inhomogeneous system then so too are the effective interactions between colloids; these do not depend on the local polymer distribution. Also we note that although the polymer degrees of freedom have been integrated out it is still possible, at least in principle, to recover information about the polymer distribution from properties that are determined by the effective Hamiltonian. For example, the polymer density $\rho_p(\mathbf{r})$ can be obtained by functional differentiation of the free energy F with respect to $V_p^{ext}(\mathbf{r})$ and expressed in terms of n-body correlation functions of the colloids, which can be determined using the effective Hamiltonian [11]. When $q < 0.1547$ this procedure yields an exact and tractable formula for the free-volume fraction $\alpha(\rho_c; z_p) \equiv \rho_p/\rho_p^r$ (the ratio of polymer density in the mixture to that in the reservoir) of a bulk fluid mixture [11].

Finally, we should remark that the one-dimensional version of the AO model, in which the colloids are modelled by hard rods and the polymer by ideal particles that are excluded from the colloids by a certain distance, can be solved *exactly* by mapping the binary mixture to an effective one-component Hamiltonian [30]. The construction of the effective Hamiltonian proceeds as in three dimensions and the effective pair potential $\phi^{eff}(X; z_p) = \phi_{cc}(X) + \phi_{AO}^{1D}(X; z_p)$, where the depletion potential ϕ_{AO}^{1D} is now the difference in accessible length for the polymers when the colloids are separated by a distance $|X|$ and when their separation is infinite. This potential is linear in $|X|$, proportional to z_p and vanishes for separations beyond the length of the polymer. Since the mapping reduces the binary mixture problem to that of a one-component fluid in one dimension, in which the particles interact via a nearest-neighbour potential, the statistical mechanics can be solved using the standard Laplace transform techniques. Results for the (osmotic) equation of state and free-volume fraction $\alpha(\rho_c; z_p)$ are given in [30], where they are compared with the corresponding results from the approximate free-volume theory.

2.2. *Density functional approach*

We have recently developed a density functional theory (DFT) for the binary AO model using the techniques of fundamental measure theory (FMT). Our new functional [16, 17] treats arbitrary size ratios q and is thus able to incorporate the effects of many body interactions which arise in the effective one-component description at larger values of q, and which represent an important feature of the model. Unlike DFT treatments of interfacial phenomena in simple fluids, where the attractive portion of the fluid–fluid pair potential is treated separately from the repulsive part in a perturbative fashion that is equivalent to a mean-field treatment (correlations are ignored) [31], here the effective attractive interactions emerge naturally from the DFT and are treated non-perturbatively. Of course, the present DFT is still mean-field like in that bulk critical fluctuations or, indeed, interfacial fluctuations are not incorporated. The excess, over ideal, Helmholtz free energy functional is given by a spatial integral over a reduced free energy density Φ which is a function of a set of species-dependent weighted densities

$$\beta\mathcal{F}_{ex}^{AO}[\rho_c(\mathbf{r}), \rho_p(\mathbf{r})] = \int d\mathbf{r}\Phi(\{n_\nu^c\}, \{n_\gamma^p\}), \tag{11}$$

where the function $\Phi = \Phi_1 + \Phi_2 + \Phi_3$ consists of three terms given by

$$\Phi_1 = n_0^c\left[-\ln(1-n_3^c) + \frac{n_3^p}{1-n_3^c}\right] - n_0^p \ln(1-n_3^c),$$

$$\Phi_2 = (n_1^c n_2^c - \mathbf{n}_1^c \cdot \mathbf{n}_1^c)\left[\frac{1}{1-n_3^c} + \frac{n_3^p}{(1-n_3^c)^2}\right] + \frac{n_1^p n_2^c - \mathbf{n}_1^p \cdot \mathbf{n}_2^c + n_1^c n_2^p - \mathbf{n}_1^c \cdot \mathbf{n}_2^p}{1-n_3^c},$$

$$\Phi_3 = \frac{(n_2^c)^3 - 3n_2^c(\mathbf{n}_2^c \cdot \mathbf{n}_2^c)}{24\pi}\left[\frac{1}{(1-n_3^c)^2} + \frac{2n_3^p}{(1-n_3^c)^3}\right] + \frac{(n_2^c)^2 n_2^p - n_2^p(\mathbf{n}_2^c \cdot \mathbf{n}_2^c) - 2n_2^c \mathbf{n}_2^c \cdot \mathbf{n}_2^p}{8\pi(1-n_3^c)^2}. \tag{12}$$

The species-dependent weighted densities are given by convolutions of the density profiles $\rho_i(\mathbf{r})$, $i = c, p$, with weight functions $w_\nu^i(\mathbf{r})$

$$n_\nu^i(\mathbf{r}) = \int d\mathbf{r}' \rho_i(\mathbf{r}') w_\nu^i(\mathbf{r} - \mathbf{r}'). \tag{13}$$

The four scalar and two vector weight functions are functions characteristic of the geometry of the hard particles

$$w_3^i(\mathbf{r}) = \Theta(R_i - r),$$

$$w_2^i(\mathbf{r}) = \delta(r - R_i),$$

$$w_1^i(\mathbf{r}) = \frac{\delta(r - R_i)}{4\pi R_i},$$

$$w_0^i(\mathbf{r}) = \frac{\delta(r - R_i)}{4\pi R_i^2},$$
$$\mathbf{w}_{v2}^i(\mathbf{r}) = \frac{\mathbf{r}}{r}\delta(r - R_i),$$
$$\mathbf{w}_{v1}^i(\mathbf{r}) = \frac{\mathbf{r}}{r}\frac{\delta(r - R_i)}{4\pi R_i}, \qquad (14)$$

where R_i denotes the radius of species i so that $R_c = \sigma_c/2$ and $R_p = \sigma_p/2$. $\Theta(r)$ is the Heaviside step function and $\delta(r)$ is the Dirac distribution.

The procedure for constructing the DFT is based on the successful FMT developed by Rosenfeld [18] for additive hard-sphere mixtures. In order to obtain the reduced free energy density Φ appropriate to the AO model, Schmidt *et al.* [16, 17] considered the zero-dimensional limit which corresponds to a cavity that can hold at most one hard-sphere colloid but can hold an arbitrary number of ideal polymers if no colloid is present. Full details of the derivation of the DFT and its applications to the determination of bulk fluid thermodynamics and structure are given in [17]. A summary is provided in section 5.1 of the present article where we consider an extension of the AO model. Here it suffices to make some remarks about the status of the theory. Note that in the original papers [16, 17] a tensor weight function was included; this contribution is omitted in the above formulation and in the calculations to be described later. Inclusion of the tensor (see equation (33) below), while essential for calculating crystalline properties, makes negligible difference for inhomogeneous fluid states and so would only serve to complicate matters without altering the basic phenomena. It is important to recognize that the functional can also be regarded as a linearization, in the polymer density $\rho_p(\mathbf{r})$, of the original Rosenfeld hard-sphere functional.

For a homogeneous fluid mixture the functional yields a reduced excess bulk free energy density

$$\beta F_{ex}^{AO}/V = \beta f_{ex}^{AO}(\rho_c, \rho_p; q) = \beta f_{ex}^{HS}(\rho_c) - \rho_p \ln \alpha(\rho_c), \qquad (15)$$

where

$$\alpha(\rho_c) = (1 - \eta_c)\exp(-A\gamma - B\gamma^2 - C\gamma^3), \qquad (16)$$

with $\gamma = \eta_c/(1 - \eta_c)$, $A = 3q + 3q^2 + q^3$, $B = 9q^2/2 + 3q^3$ and $C = 3q^3$. f_{ex}^{HS} is the excess free energy density of pure hard spheres in the scaled particle (PY compressibility) approximation; an explicit expression is given later in equation (36). This result can be shown to be identical to the free-volume theory of Lekkerkerker *et al.* [4, 10], where $\alpha(\rho_c)$ is interpreted as the ratio of the free volume accessible to a single test polymer sphere and the system volume. It is not immediately obvious that the DFT approach should be equivalent to free-volume theory. The starting points for the two theories are quite different and it is usually the semi-grand free energy that is considered in free-volume theory; connections between the two approaches are discussed in [17]. Free-volume theory treats the semi-grand free energy as the sum of a hard-sphere (colloid) part plus a contribution from an ideal gas of polymers in the free volume left by the colloids, which is treated as an expansion in the fugacity z_p truncated at the term linear in z_p [4, 10]. This linearity in z_p, or equivalently in ρ_p, is built into the DFT.

The bulk pair direct correlation functions $c_{ij}^{(2)}$, obtained by taking two functional derivatives of $\mathcal{F}_{ex}^{AO}[\rho_c, \rho_p]$, are given analytically [17]. The Ornstein–Zernike relations then provide the partial structure factors $S_{ij}(k)$. Linearization in the polymer density has the consequence that $c_{pp}^{(2)} = 0$, as in the PY approximation for this AO model. However, the other direct correlation functions $c_{cc}^{(2)}$ and $c_{cp}^{(2)}$ are *not* the same as those from PY approximation, even though $c_{ij}^{(2)}(r)$ vanishes for $r > R_i + R_j$ in both the DFT and the PY treatments. In an exact treatment we would expect contributions to $c_{ij}^{(2)}(r)$ beyond $R_i + R_j$. An important advantage of the DFT over integral equation theories is that the partial structure factors and radial distribution functions $g_{ij}(r)$ obtained from the Ornstein–Zernike equations yield a spinodal consistent with that from the bulk free energy (15), i.e. the free-energy and structural routes to the fluid–fluid spinodal are consistent. (Note that the spinodal can be obtained *analytically* from the canonical free energy (15)—see [17].) Such a property is especially advantageous when considering interfacial properties at or near two-phase coexistence. Schmidt *et al.* [17] also investigate the asymptotic decay, $r \to \infty$, of $g_{ij}(r)$ in different regions of the bulk phase diagram. Since the partial structure factors $S_{ij}(k)$ are given analytically it is straightforward to determine the poles of these functions in the complex plane and hence locate the so-called Fisher–Widom line [32–35] where the ultimate decay of $rg_{ij}(r)$ crosses over from oscillatory to purely monotonic, exponential decay. Examples of the cross-over lines and of (mean-field) critical point behaviour of $S_{ij}(k)$ for various size ratios q are given in [17].

It is important to emphasize that, within the framework of DFT, the Ornstein–Zernike route is not the only one to the pair correlation functions. The alternative is the test particle route, whereby one fixes a particle of species i at the origin and determines (by solving the appropriate Euler–Lagrange equations, obtained by minimizing the functional) the inhomogeneous one-body density profile $\rho_j(r)$ arising from the external potential exerted by the fixed particle i; then $g_{ij}(r) = \rho_j(r)/\rho_j(\infty)$. All that is required to solve the

relevant equations are the one-body direct correlation functions $c_i^{(1)}(r)$, which involve only a first derivative of $\mathcal{F}_{ex}^{AO}$. One can show that in the limit $\eta_c \to 0$, the test particle route for the DFT yields the exact result $g_{cc}(r) \approx \exp(-\beta\phi^{eff}(r; z_p))$, where ϕ^{eff} is the effective depletion potential defined in equation (6) [16, 17]. In other words, the geometrically based DFT describes correctly the depletion effect between two hard-sphere colloids when implemented within the test-particle procedure. There are other good reasons to believe that the test-particle route to $g_{ij}(r)$ should be more accurate than the Ornstein–Zernike route [17].

3. The fluid–fluid interface

Phase separation in the AO model is a well-studied problem [4, 8–10]. As remarked earlier, for small size ratios q, fluid–fluid phase separation is pre-empted by a fluid–solid transition so the former is, at best, metastable. For larger values of q, however, there is stable, entropically driven, fluid–fluid phase separation. Free-volume theory for the AO model predicts stable liquid (colloid-rich)–gas (colloid-poor) phase coexistence for $q > 0.32$. It follows that our present DFT predicts the same behaviour. Figure 2 shows the bulk phase diagram obtained from the present theory for a size ratio $q = 0.6$ for which there is a stable fluid–fluid demixing transition with a critical point at $\eta_{p,crit}^r \sim 0.495$. The polymer reservoir packing fraction is defined as $\eta_p^r = (\pi/6)\sigma_p^3\rho_p^r$,

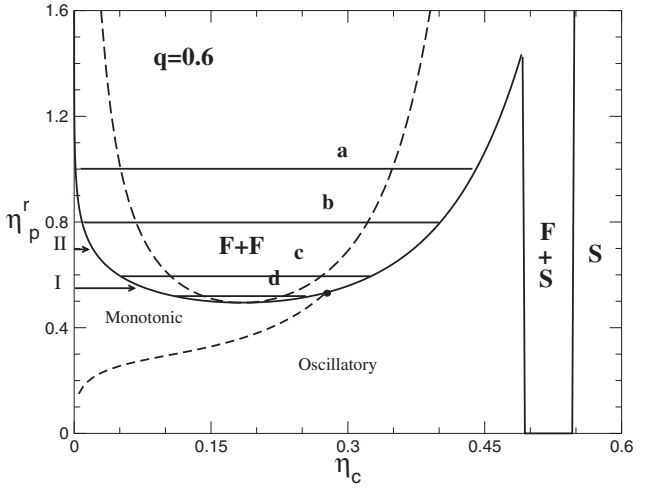

Figure 2. The bulk phase diagram calculated from the functional for $q = 0.6$. η_c is the packing fraction of the colloid and η_p^r that of polymer in the reservoir. F denotes fluid and S solid. The long dashed line shows the fluid–fluid spinodal and the short dashed line shows the Fisher–Widom line. The latter intersects the binodal at $\eta_{p,FW}^r = 0.53$. The horizontal tie lines (a), (b), (c) and (d) connect coexisting fluid states. Horizontal arrows indicate the paths I and II by which the phase boundary is approached for the adsorption studies in section 4.2.

with $\rho_p^r = z_p$ for ideal polymer. Note that the tie lines connecting coexisting states are horizontal in this (reservoir) representation. It should be emphasized that the fluid–fluid and fluid–solid phase boundaries presented here are those of the original free-volume theory [4, 10]†. While the fluid–fluid phase boundary shown is precisely that given by the functional, the true solid–fluid boundary from DFT would require a full minimization of the functional for a solid-like distribution. This is outside the scope of the present study. Also shown in figure 2 is the Fisher–Widom (FW) line which divides the phase diagram into regions where the asymptotic decay of the three bulk pairwise correlation functions, $rg_{ij}(r)$, is either monotonic or exponentially damped oscillatory. The FW line has important consequences both for our study of the free fluid–fluid interface and for adsorption at a wall as the asymptotic behaviour predicted for the bulk pair correlations applies also to the one-body density profiles [33, 34].

We turn now to the free interface between demixed fluid phases. The density profiles for colloid and polymer are obtained by minimizing the grand potential functional

$$\Omega[\rho_c(\mathbf{r}), \rho_p(\mathbf{r})] = \mathcal{F}_{id}[\rho_c(\mathbf{r}), \rho_p(\mathbf{r})] + \mathcal{F}_{ex}^{AO}[\rho_c(\mathbf{r}), \rho_p(\mathbf{r})] + \sum_{i=c,p} \int d\mathbf{r}(V_i^{ext}(\mathbf{r}) - \mu_i)\rho_i(\mathbf{r}) , \qquad (17)$$

where $\mathcal{F}_{ex}^{AO}$ is the excess Helmholtz free energy functional of the AO mixture given in equation (11), $\mathcal{F}_{id}$ denotes the functional for the ideal mixture, μ_i is the chemical potential (fixed by the reservoir) and $V_i^{ext}(\mathbf{r})$ is the external potential coupling to species i with $i = c, p$. In the case of the free interface $V_i^{ext} \equiv 0$. The fact that the functional is linear in the polymer density makes solution of the AO Euler–Lagrange equations considerably simpler than for the more familiar binary hard-sphere Rosenfeld functional [18]. In the latter case, the two minimization conditions $\delta\Omega/\delta\rho_1 = 0$ and $\delta\Omega/\delta\rho_2 = 0$ give rise to two coupled equations for ρ_1 and ρ_2 which must be solved self-consistently. The AO functional can be minimized explicitly with respect to the polymer density and the level of computational complexity reduced to that of minimizing a functional with respect to a single density field [17].

The colloid density profiles and corresponding surface tensions are shown in figure 3. The surface tension is plotted here in $\mu N\,m^{-1}$ to facilitate comparison with the experimental results of [36, 37] which we shall

†Note that in calculations, e.g. [10], based on free volume theory the Carnahan–Starling approximation is often used for f_{ex}^{HS} whereas in DFT the PY compressibility approximation must be employed.

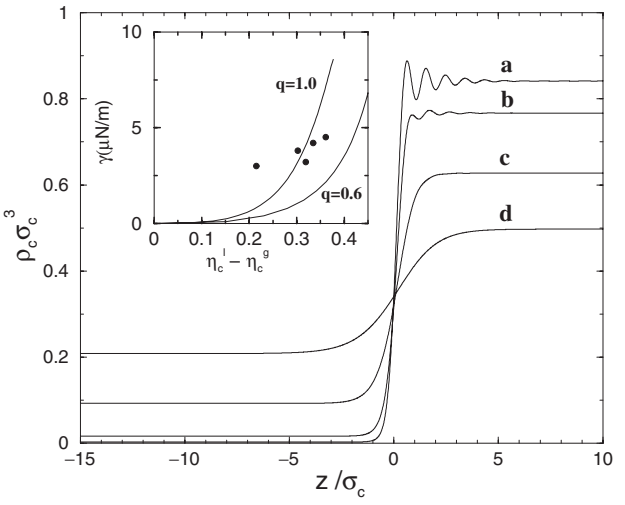

Figure 3. Colloid density profiles at the free interface between demixed fluid phases for a size ratio $q = 0.6$. The polymer reservoir packing fractions correspond to the tie lines in figure 2, i.e. $\eta_p^r = 1.0$ (a), 0.8 (b), 0.6 (c) and 0.52 (d) (near critical point). States (a), (b) and (c) lie on the oscillatory side of the FW line. The inset shows the surface tension γ versus the difference in the colloidal packing fraction in coexisting liquid (l) and gas (g) phases for $q = 0.6$ and 1.0. The colloid diameter is taken to be 26 nm to compare with experimental data of [36] (points) where $q = 1.0$.

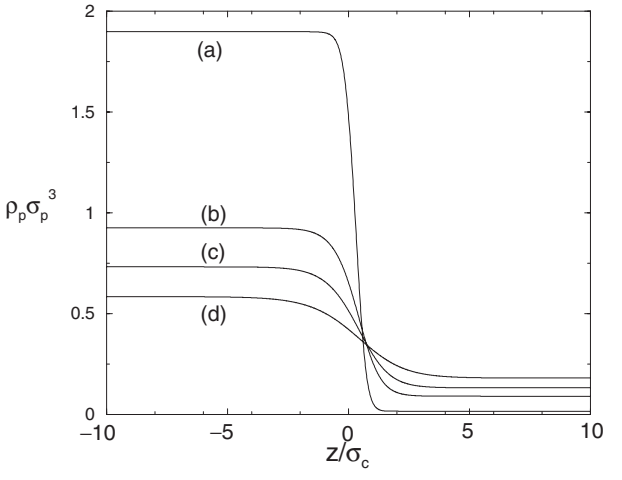

Figure 4. Polymer density profiles for $q = 0.6$ corresponding to the colloid profiles shown in figure 3. The polymer reservoir packing fractions correspond to the tie lines in figure 3, i.e. $\eta_p^r = 1.0$ (a), 0.8 (b), 0.6 (c) and 0.52 (d) (near critical point). States (a), (b) and (c) lie on the oscillatory side of the FW line.

return to later but which correspond to size ratio $q \sim 1$, i.e. we take the colloid diameter to be 26 nm in accordance with the experiments. The polymer profiles are given in figure 4 and demonstrate the polymer partitioning between the two phases. We show four profiles for states between the critical and triple points. The labels (a)–(d) in figure 3 correspond to the tie lines in figure 2; (d) corresponds to the free interfacial profiles between coexisting densities near to the critical point and (a) to a near triple point state. For state (d) the colloid profile is smooth and reminiscent of the profiles of [38] calculated using an effective one-component Hamiltonian and employing a square gradient functional. For states approaching the triple point the interfacial width is found to be approximately σ_c, similar to values inferred from ellipsometric measurements on a colloid–polymer mixture [39] where a tan h function was fitted to the refractive index profile through the interface.

While the profiles near the critical point are smooth and rather unsurprising, for states nearer to the triple point striking oscillations develop on the colloid-rich 'liquid' side of the profiles. Such oscillations have been found previously in theoretical studies [33] of the free liquid–vapour interface of the square-well fluid and in simulation studies of the liquid–liquid interface [40] in a simple model of a liquid mixture. The presence of oscillations in one-body density profiles at interfaces is intimately connected to the asymptotic decay of bulk pairwise correlations [33, 34]. For the present mixture oscillatory profiles arise at the free interface when the colloid density in the coexisting liquid is greater than the colloid density where the FW (Fisher–Widom) line intersects the binodal, i.e. for all states with $\eta_p^r > \eta_{p,FW}^r = 0.53$ for $q = 0.6$—see figure 2. The general theory of asymptotic decay of correlations in mixtures with short-range forces predicts [33, 34] that the longest-range decay of the density profiles should be

$$\rho_i(z) - \rho_i \sim \rho_i A_i \exp(-\alpha_0 z), \quad z \to \infty, \tag{18}$$

on the monotonic side of the FW line and

$$\rho_i(z) - \rho_i \sim \rho_i \tilde{A}_i \exp(-\tilde{\alpha}_0 z) \cos(\alpha_1 z - \theta_i), \quad z \to \infty, \tag{19}$$

on the oscillatory side; ρ_i is the bulk density of species i. Equivalent definitions exist for $z \to -\infty$, with appropriate bulk densities ρ_i. On the FW line, $\alpha_0 = \tilde{\alpha}_0$. The decay lengths α_0^{-1} and $\tilde{\alpha}_0^{-1}$ and the wavelength of oscillatory decay $2\pi/\alpha_1$ are common to both species and are properties of the bulk fluid. These are determined by the (common) poles of the structure factors $S_{ij}(k)$ [34]. The amplitudes A_i, $\tilde{A}_i$ and the phase θ_i are species dependent and although there is knowledge about the amplitude *ratios* in binary mixtures [34], there is no theory for the absolute amplitude of the oscillations. We have confirmed that for states where the colloid profile oscillates, the corresponding polymer profiles also exhibit oscillations on the same, colloid-rich side

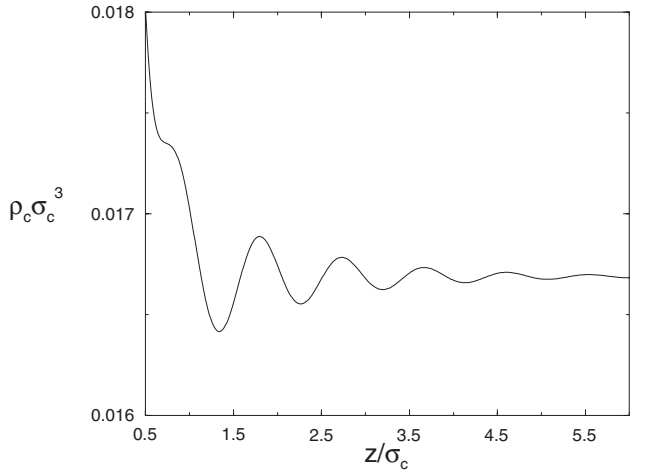

Figure 5. An enlargement of the polymer profile for $q = 0.6$ and $\eta_p^r = 1.0$, i.e. state (a) shown in figure 4. The oscillations, although not visible on the scale of figure 4, are present in the polymer profiles and display the same period and decay length as the corresponding colloid profiles (figure 3).

of the interface, with identical wavelength and decay length to those of the colloid. As the bulk density of the polymer is low in the colloid-rich 'liquid' phase, the amplitude of the polymer oscillations is very small; figure 5 shows an enlargement of the oscillations in the polymer profile for state (a). For states just above the FW intersection point, $\eta_{p,FW}^r$, the amplitude of the colloid oscillations can also become extremely small and this is why the profile (c) does not show oscillations on the scale of figure 3. For state (a), with $\eta_p^r = 1$, which is not especially close to the estimated triple point, the amplitude of the oscillations is substantial and appears to be larger than the corresponding amplitude for a square-well fluid very near its triple point where the oscillations have a wavelength of about one atomic diameter [33]. Our present results resemble closely those of a recent DFT treatment of binary mixtures of repulsive Gaussian core particles which exhibit fluid–fluid phase separation [41], although in that case there are states for which oscillations occur on both sides of the interface.

We note that all DFT treatments are mean-field-like in that they ignore fluctuation effects, both of the bulk liquid (critical fluctuations) and of the interface. Thermally induced capillary wave fluctuations of the interface will act to erode the oscillations in the 'bare' (mean-field) density profiles but it is argued that at least some of the oscillatory structure will remain in the 'dressed' colloid profiles. The standard method of incorporating capillary wave fluctuations is to assume that DFT calculations yield a 'bare' or 'intrinsic' profile and that interfacial fluctuations can be 'unfrozen' by an appropriate renormalization of the mean-field profile [31, 33, 34, 42]. Because of the extremely low surface tensions γ which occur in colloidal systems one might expect the oscillations to be completely washed out by inclusion of these fluctuation effects but we will argue that this is not necessarily the case. In the simplest treatment of capillary wave fluctuations the intrinsic interface is smeared by a Gaussian convolution over the interfacial thermal roughness $\xi_\perp$. For oscillatory profiles which decay as equation (19) the wavelength and decay length are unaltered by this convolution but the amplitude is reduced by a factor $\exp[-(\alpha_1^2 - \tilde{\alpha}_0^2)\xi_\perp^2/2]$ [33, 34, 42]. The roughness $\xi_\perp$ depends upon both the interfacial area L^2 and the external potential, i.e. the Earth's gravitational field. For zero gravitational field, $\xi_\perp^2 = (2\pi\beta\gamma)^{-1} \ln(\Lambda_{max}/\Lambda_{min})$, where Λ_{max} and Λ_{min} are upper and lower cut-off wavenumbers for the capillary wave fluctuations. If we choose $\Lambda_{max} = 2\pi/\xi$ and $\Lambda_{min} = 2\pi/L$, where $\xi = \tilde{\alpha}_0^{-1}$ is the correlation length of the bulk coexisting 'liquid' phase, it follows that the amplitude of the oscillations in the density profile will be reduced by a factor

$$\tau = (L/\xi)^{-\omega[(\alpha_1/\tilde{\alpha}_0)^2 - 1]}, \tag{20}$$

where we have introduced the dimensionless parameter

$$\omega = \frac{k_B T}{4\pi\gamma\xi^2}, \tag{21}$$

which measures the strength of the capillary wave fluctuations. Smaller surface tensions give rise to larger values of ω and, as a result, the amplitude of the oscillations is damped more severely. Molecular dynamics simulations of a liquid–liquid interface have been performed by Toxvaerd and Stecki [40]. These authors (see also Chacón and co-workers [43, 44] who performed Monte Carlo simulations of the liquid–gas interface of a model of a metal) found a decrease in the amplitude of oscillation with increasing L, consistent with a Gaussian renormalization of the oscillatory intrinsic interface. We find for the present model that ω takes values of a similar order of magnitude as those for simple fluids [38]. This is due to the fact that the bulk correlation length ξ scales roughly as σ_c [16, 17] and the tension γ as $k_B T/\sigma_c^2$ [38, 45]. From our explicit calculations of γ and ξ we find that at state point (a), for which the profile has pronounced oscillations, see figure 3, $\tilde{\alpha}_0\sigma_c = 0.77$, $\alpha_1\sigma_c = 6.74$ and the reduced surface tension $\gamma^* = \beta\gamma\sigma_c^2 = 1.13$ which implies that $\omega = 0.042$ and $(\alpha_1/\tilde{\alpha}_0)^2 - 1 = 75.12$. We thus find that $\tau = (L/\xi)^{-3.23}$ which suggests that detecting oscillations of the colloid profile should be no more difficult than for simple fluids where the exponent is expected to take

a similar value. Indeed, from an experimental viewpoint such oscillations in a colloidal system offer an interesting opportunity for experimental study as it should be more favourable to investigate such structuring in systems where the period is of colloidal size than in atomic fluids, where the period is on the Angström scale.

We conclude this section by returning to the results for the surface tension. The inset in figure 3 shows the tension γ for size ratios $q = 0.6$ and 1.0. We find that the tension calculated using the present DFT is consistently larger than that calculated [38] using the effective one-component Hamiltonian treated by square gradient DFT. The level of agreement with the experimentally measured tension for mixtures of a silica colloid, coated with 1-octadecanol, and polydimethylsiloxane (PDMS) in cyclohexane at $T = 293$ K [36] is somewhat better than in [38]. The size ratio for this mixture is approximately 1.0. As mentioned earlier, in order to compare our DFT results with experiment we choose $\sigma_c = 26$ nm, the mean diameter of the particles investigated in [36]; there are no adjustable parameters in the model [25, 26, 46].

Note that the measured tensions are typically 3–4 μN m^{-1}, values which are about 1000 times smaller than the tensions measured for simple atomic fluids near their triple points. Such small values of the tension are not so surprising when one recalls (i) that the tension scales roughly as k_BT/σ_c^2, provided the state is well removed from the critical point and (ii) that $\sigma_c \sim 100$ atomic diameters [38, 45]. In figure 3 the tension is plotted against the difference between η_c in the coexisting liquid (l) and gas (g) phases. Within the present mean-field treatment γ vanishes as $(\eta_c^l - \eta_c^g)^3$ on approaching the critical point. Incorporating critical fluctuations should lead to even faster decay; for Ising-like criticality the exponent 3 should be replaced by $2\nu/\beta \approx 3.9$. The experiments of [36] were not performed sufficiently close to the critical point to examine scaling behaviour. However, Chen *et al.* [47] do report results for the density difference and surface tension, in a similar mixture of silica particles and PDMS in cyclohexane, taken near the critical point. They report values for $\gamma < 1\,\mu$N m^{-1} and a good fit to Ising-like scaling.

4. Adsorption at a hard wall

In this section we consider the AO mixture adsorbed at a planar hard wall described by the external potentials (8). Such a model constitutes the simplest framework in which one can address the statistical mechanics of colloidal adsorption or, more specifically, the effects of entropic depletion forces on the distribution of both colloids and polymer near a (repulsive) substrate. Of course, other more complex wall–fluid potentials can be considered which include soft repulsion and/or attractive interactions. The advantages of the hard-wall model are (i) it encompasses the key feature of depletion-induced wall–colloid attraction and (ii) as emphasized in section 2.1, it can be mapped exactly to a very simple effective Hamiltonian (9), for $q < 0.1547$, that can be used efficiently in simulation studies.

We focus first on the case $q = 0.1$, for which there are Monte Carlo results [11] for the colloid density profile against which we can test the reliability of our DFT. Afterwards we consider larger size ratios where bulk fluid–fluid phase separation occurs. This enables us to investigate entropic wetting phenomena at the hard wall using the DFT approach.

4.1. *Test case:* $q = 0.1$

In order to test the performance of the DFT for adsorption studies we first calculate density profiles against a hard wall for $q = 0.1$. For this small size ratio, simulation results are available [11] for the colloid profiles. These make use of the exact mapping to the effective Hamiltonian (9); only a pairwise additive fluid–fluid potential (ϕ_{AO}) and an explicit one-body wall–fluid depletion potential (ϕ_{AO}^{wall}) are involved. As previously, we minimize the functional (17) but now for a hard wall with external potentials (8). The results obtained from the present DFT (figure 6) should be compared and contrasted with those of [11] where the effective one-component Hamiltonian was treated by means of a one-component mean-field DFT which treats the hard-sphere contribution by Rosenfeld's FMT and the attractive contribution, arising from $\phi_{AO}(R)$, in mean-field fashion. We find that the present mixture functional provides an equally good description of the colloid profiles, in particular the dramatic increase in the wall contact value, $\rho_c(\sigma_c^+/2) \equiv \rho_{wc}$, as polymer is added; the present functional clearly incorporates the depletion attraction between the wall and the colloids. It should be noted that the binary mixture AO functional generates internally all depletion effects between the colloids and between the colloids and the hard wall, whereas in the previous one-component treatment these are essentially put in by hand. We choose polymer reservoir packing fractions $\eta_p^r = 0.05$ and $\eta_p^r = 0.1$ and a fixed bulk colloid packing of $\eta_c = 0.3$, as Monte Carlo simulation results exist for these state points. We intentionally stay away from the vicinity of the solid–fluid phase boundary which is at about $\eta_p^r = 0.16$ [10].

The present functional tends to give significantly more structured colloid profiles than does the effective one-component DFT of [11]. In fact it appears that the binary mixture AO DFT consistently overestimates the degree of structuring (more pronounced maxima and minima than in simulation) whereas the one-component DFT gives an underestimate. When there is no polymer

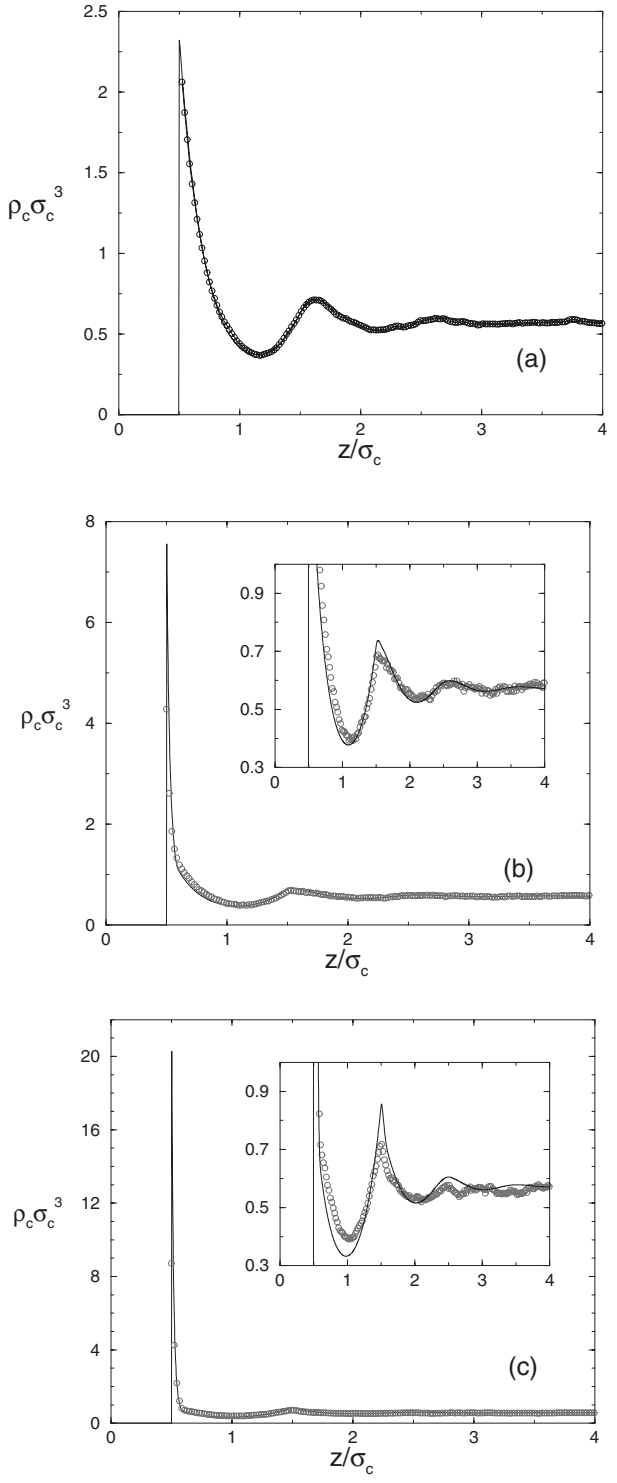

Figure 6. The colloid density profiles calculated from the binary mixture DFT compared with simulation results for a size ratio $q = 0.1$ and bulk colloid packing fraction $\eta_c = 0.3$. The packing fractions of the polymer reservoir are (*a*) $\eta_p^r = 0$ (hard spheres), (*b*) 0.05 and (*c*) 0.10, respectively. The circles are the Monte Carlo results [11] and the solid lines are the DFT results. The insets show the results on an expanded scale. Note the rapid increase in the density near contact as η_p^r is increased.

in the system, $\eta_p^r = 0$, see figure 6 (*a*), both functionals reduce to the Rosenfeld functional for pure hard spheres and, as is well known, this performs very well for the full range of bulk packing fractions. The oscillations arise from packing effects at the hard wall.

On adding a small amount of polymer, $\eta_p^r = 0.05$, there is a pronounced increase in the contact value, figure 6 (*b*), as a result of the wall-induced depletion which is now implicitly incorporated into the mixture DFT. We obtain a contact value of $\rho_{wc}\sigma_c^3 \sim 7.56$ which is slightly higher than the value 6.41 obtained from the effective one-component DFT [11]. For such small size ratios the wall–colloid depletion potential is strongly attractive and of short range ($0.1\sigma_c$) and it thus becomes difficult to achieve good simulation statistics close to the wall [11]. The simulation results have been extrapolated to contact and yield a value $\rho_{wc}\sigma_c^3 \sim 4.28$. For $\eta_p^r = 0.1$, see figure 6 (*c*), the wall–colloid depletion attraction becomes even stronger and the present DFT gives a contact value $\rho_{wc}\sigma_c^3 \sim 20.29$; again this is larger than the corresponding result from the one-component functional, which is 15.52. Note that these very high values of the local density decay to roughly unity over the range of the wall–colloid depletion potential, i.e. $0.1\sigma_c$. The insets in figures 6 (*b*) and 6 (*c*) show that the DFT captures correctly the non-trivial 'triangular' structure of the second peak in the profile but for both $\eta_p^r = 0.05$ and 0.1 the first minimum is deeper than the simulation result and the height of the second maximum is overestimated. As η_p^r is increased the oscillations become damped more rapidly and $\rho_c(z)$ is close to the bulk value after a distance of approximately $4\sigma_c$. Numerical results were checked using the hard wall sum rule, $\beta P = \rho_c(\sigma_c^+/2) + \rho_p(\sigma_p^+/2)$, where P is the total pressure [11]. Recall that for each colloid profile we present here we also have the corresponding polymer profile. The sum rule was satisfied to better than 0.1% in all cases. It should be noted that comparing the DFT results with those of simulation for such a highly asymmetric mixture constitutes a severe test. The fact that the AO mixture DFT performs well under such difficult conditions is thus most encouraging. In addition, the free-volume theory, which gives a bulk free energy (15) identical to that of the AO functional, becomes increasingly accurate for larger q values. We might reasonably expect the performance of the functional to improve accordingly. Although the bulk free energy obtained from the functional improves with increasing q, this does not guarantee that one-body profiles will be any better. Nevertheless, since the profiles obey the hard wall sum rule, the contact values should become closer to those of simulation as q increases, in accordance with the increasing accuracy of the free-volume bulk pressure. These considerations are relevant

when we focus on larger size ratios ($q > 0.32$) where stable fluid–fluid demixing occurs and investigate interfacial phase transitions at the hard wall–fluid interface.

The physical significance of the simulation results for $q = 0.1$ were discussed in [11] and we do not dwell upon this here. Rather we simply emphasize that since the colloid density profiles decay so rapidly from their very high contact densities over the short range of the wall–fluid depletion potential, ϕ_{AO}^{wall}, the amount of colloid adsorbed in the contact 'layer' is rather small (fraction of a monolayer). Indeed the Gibbs adsorption of colloid does not increase rapidly with increasing η_p^r [11]. From examination of the one-body profiles and simulation snapshots there was no evidence of wall-induced local crystallization at the polymer concentrations we examined. However, the state points we considered were still well removed from the bulk fluid–solid phase boundary. The issue of when and how wall-induced crystallization occurs is an important one, both conceptually and because there are several experimental papers reporting evidence for the phenomenon (in colloid–colloid as well as in colloid–polymer mixtures) occurring for state points well below the bulk phase boundary—see [11] for a summary.

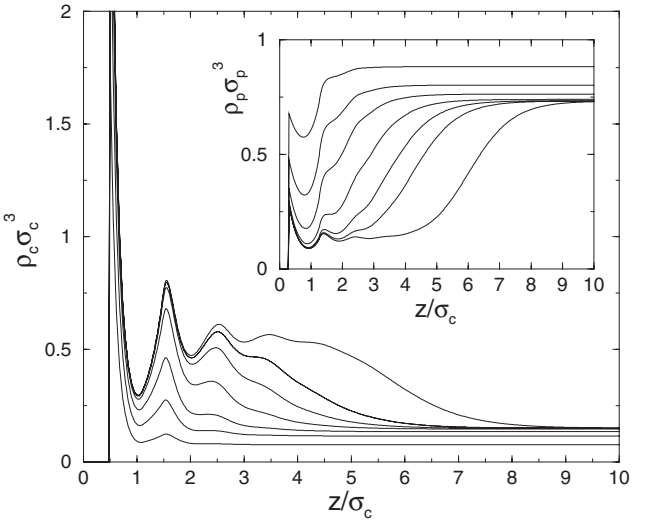

Figure 7. Colloid density profiles for $q = 0.6$ showing the onset of complete wetting of a hard wall by the colloid-rich phase at $\eta_p^r = 0.55$ as the bulk phase boundary is approached along path I in figure 2. Bulk colloid fractions are $\eta_c = 0.04$, 0.06, 0.07, 0.076, 0.0775, 0.0778 and 0.0779 (from bottom to top). The coexisting gas density is $\eta_c = 0.078\,12$. The inset shows the polymer profiles for the same values of η_c (from top to bottom). Note that the polymer distribution becomes progressively more depleted as the colloid-rich layer grows in thickness.

4.2. *Entropic wetting and layering:* $q \geq 0.6$

For these larger size ratios the bulk phase diagram exhibits three stable phases, as in figure 2. In determining the adsorption characteristics, we choose to fix η_p^r and approach the bulk fluid–fluid phase boundary from the colloid poor side. This is analogous to performing a gas adsorption isotherm measurement for a simple atomic fluid, recalling that η_p^r plays a role equivalent to inverse temperature in the AO model. Depending on the value of η_p^r chosen, we find the adsorption behaviour changes dramatically. For the present AO model one might expect to observe similar behaviour as that pertaining to simple fluids adsorbed at attractive substrates; we have a system of colloids interacting via an effective Hamiltonian which gives rise to fluid–fluid phase separation in bulk and a depletion induced attraction acting between the colloids and the wall. However, in the present case we have effective many-body colloid–colloid and many-body wall–colloid potentials for the size ratios of interest, i.e. values of q large enough to give rise to a stable bulk fluid–fluid transition. For large size ratios the effective wall–colloid potential ceases to be a simple one-body potential acting on individual colloids and becomes a complicated function of multiple colloid coordinates. We find that these complex wall potentials do indeed give rise to new phenomena which are quite distinct from those seen in simple fluids. As an example we consider size ratio $q = 0.6$ and describe some of the phenomena encountered as we increase η_c, for fixed η_p^r, towards the bulk phase boundary. We consider, in turn, paths I and II shown in figure 2.

We first choose a path just above the critical point, $\eta_p^r = 0.55$, i.e. follow path I in figure 2. The layer of liquid-like colloid density grows continuously against the wall and becomes macroscopically thick as the phase boundary is approached. The colloid density profiles in figure 7 show the onset of complete wetting by the colloid-rich phase. We have confirmed that for states with smaller values of η_p^r (but above the critical value $\eta_{p,crit}^r$) the equilibrium film thickness, t_{eq}, or, equivalently, Γ_c, the adsorption of colloid, grows logarithmically with the deviation from the bulk phase boundary. Although a detailed investigation of the amplitude was not performed this should be the bulk correlation length of the wetting (colloid-rich) phase, as is appropriate to a system where all the interactions are of finite range—see e.g. [48]. The corresponding polymer profiles are shown in the inset and indicate how polymer becomes more depleted as the colloid-rich layer grows; the polymer can be effectively regarded as a 'slave' species with profiles determined by the distribution of colloid [17]. Strictly speaking, *macroscopically* thick wetting films can only occur when the density of coexisting liquid lies on the monotonic side of the

FW line in figure 2, i.e. for $\eta_p^r < \eta_{p,FW}^r$, the point of intersection of the FW line and the binodal. One can envisage a coarse grained description of wetting phenomena whereby the surface excess free energy can be regarded as an effective wall or binding potential, $\Phi_{wall}(t)$, acting on a single degree of freedom, the film thickness t [49]. For $\eta_{p,crit}^r < \eta_p^r < \eta_{p,wet}^r$ and $\eta_p^r < \eta_{p,FW}^r$ the potential $\Phi_{wall}(t)$ exhibits a single minimum at a finite equilibrium film thickness t_{eq} provided the state is off bulk coexistence. $\eta_{p,wet}^r$ denotes the polymer reservoir packing fraction at the wetting transition. As the value of η_c is increased towards coexistence the position of this minimum, and hence t_{eq}, increases continuously to infinity. If we are in the region where $\eta_{p,crit}^r < \eta_p^r < \eta_{p,wet}^r$ and $\eta_p^r > \eta_{p,FW}^r$ the decay of the density profiles is oscillatory. It can be shown [50] that in this region the effective binding potential $\Phi_{wall}(t)$ possesses a corresponding oscillatory decay. As a result the minimum, t_{eq}, of the binding potential will always lie at a finite value. Such oscillatory binding potentials will stabilize very thick but finite films, which would otherwise be infinite, even at bulk coexistence. This is because the global minimum lies at the trough of one of the oscillations and not at infinity. Such situations can easily lead to numerical difficulties when using iterative methods because of the presence of a large number of metastable minima and care must be taken to ensure that the global minimum of the excess (over bulk) free energy is reached. By choosing $\eta_p^r = 0.55$ we avoid many of these complications and can easily obtain films of thickness 20 or $30\sigma_c$. We confirmed that in the flat portion of the profiles the densities of colloid and polymer are equal to their values in the coexisting colloid-rich phase. In order to investigate such thick wetting films it is necessary to work very close to bulk coexistence and solving the Euler–Lagrange equations resulting from minimizing the functional can be very slow.

Very different scenarios arise for other paths approaching bulk coexistence. As η_c is increased along path II, see figure 2, at fixed $\eta_p^r = 0.7$ the colloids behave essentially as an ideal gas in the presence of the wall–colloid depletion potential but with some enhancement of the contact value due to packing effects. A selection of profiles calculated along this path is shown in figure 8. The profiles remain largely unstructured until $\eta_c = 0.0198$ where a first-order phase transition occurs and a second liquid-like layer is adsorbed against the wall. The inset to figure 8 shows the discontinuous jump in the (reduced) Gibbs adsorption of the colloids, Γ_c, at the transition. The Gibbs adsorption is defined as

$$\Gamma_c = \sigma_c^2 \int_0^\infty dz\,(\rho_c(z) - \rho_c(\infty)), \qquad (22)$$

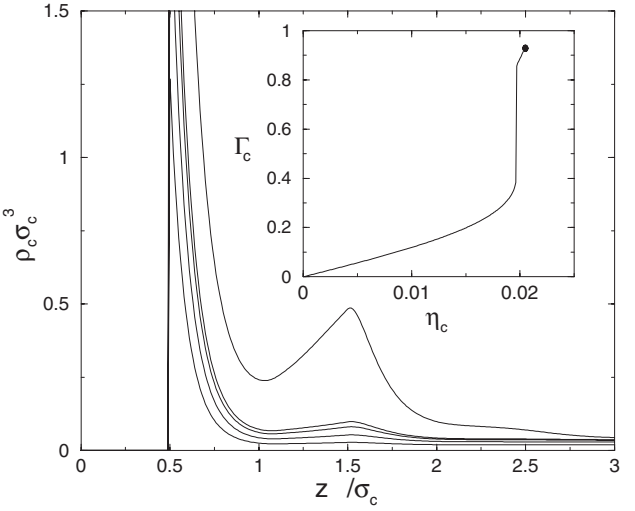

Figure 8. Colloid density profiles for size ratio $q = 0.6$ showing the first layering transition at $\eta_p^r = 0.7$ corresponding to path II in figure 2. Bulk colloid fractions are $\eta_c = 0.010$, 0.015, 0.018, 0.019 and 0.020 (from bottom to top); the transition occurs between 0.019 and 0.020. The inset shows the corresponding jump in the Gibbs adsorption Γ_c. Γ_c remains finite at bulk coexistence $\eta_c = 0.0203$, i.e. the interface is partially wet by the colloid-rich phase.

where $\rho_c(\infty)$ is the density of colloid in the bulk. This layering transition is most unusual and is quite different from the transitions between layered liquid-like films found in DFT studies of simple fluids at attractive substrates—see e.g. [51] which considers a Yukawa fluid against an attractive Yukawa wall. The transitions found in [51] are for temperatures very close to the triple point and the sequence always leads to complete wetting at coexistence. In the present case we are far away from the free volume triple point at $\eta_p^r \sim 1.43$ (although its location within a full DFT treatment of the solid is not known). Moreover the transition is to only a single extra layer; the adsorption remains finite all the way to coexistence. Thus the wall is partially wet for this value of η_p^r. Since for $\eta_p^r = 0.7$ the wall is partially wet, whereas for $\eta_p^r = 0.55$ the wall is completely wet, we can infer that there exists an analogue of the wetting transition temperature, i.e. there is a wetting polymer reservoir packing fraction $\eta_{p,wet}^r$, at which along coexistence there is a transition from partial wetting to complete wetting. It should be noted that when the second layer is adsorbed its density is not that of the coexisting liquid, rather it is at some lower liquid-like density. For values of η_c away from the layering transition, numerical solution of the Euler–Lagrange equations is extremely rapid due to the very low bulk density of colloid. As the transition is approached convergence slows considerably and large numbers of iterations are required to overcome the free energy barrier separating layered

and unlayered profiles. In the sequence of layering transitions calculated in [51] the appearance of layer n is accompanied by a jump of density in the preceding layers, primarily effecting the $(n-1)$th layer. The jump in adsorption which occurs at the transition thus receives a contribution from all layers, not only layer n. A similar effect can be seen at the present layering transition where the first contact peak in the colloid profile jumps as a second layer is adsorbed.

The layering transition which we find from the AO functional, distinct from the wetting transition, appears to result from effective many-body wall–fluid and fluid–fluid potentials acting on the colloids. It does not appear to have a direct counterpart in the adsorption of simple fluids—see section 7. In order to test this assertion we have calculated colloid density profiles using the mean-field DFT employed in [11]. As described in the previous subsection, we treat the AO pair potential as a mean-field perturbation to a hard sphere reference system and apply an external potential consisting of a hard wall plus the one-body AO wall–colloid potential, see equation (9). We find that whilst a wetting transition does exist, there is no sign of the layering which we obtain from the AO mixture DFT. The phase boundary was approached for different fixed values of η_p^r above $\eta_{p,\,wet}^r$. In each case the adsorption was found to increase *smoothly* to a finite value at bulk coexistence.

In order to map out the full interfacial diagram and locate further layering transitions we calculate density profiles *along* the coexistence curve starting at large values of η_p^r working down towards the critical point, $\eta_{p,\,crit}^r$. Using the transition points (jumps) on the phase boundary as a guide we then take slices across the phase diagram, increasing η_c for a fixed value of η_p^r, so we can locate any lines of first-order transitions which may extend into the single phase (dilute in colloid) region. We have determined interfacial phase diagrams for size ratios $q = 0.6, 0.7$ and $q = 1.0$ in order to identify any variation of the topology with size ratio. Figure 9 shows the interfacial phase diagram for $q = 0.6$; it is very rich and features not only the wetting and first layering transitions discussed above but also two further layering transitions. Figure 10 shows the colloid density profiles calculated along the bulk coexistence curve for a number of values of η_p^r and the corresponding adsorption Γ_c is shown in figure 11. Since these layering transitions are rather unusual we give a brief description of how they are located.

We begin mapping out the phase diagram by calculating the profiles at coexistence for large η_p^r, region (a) in figure 9. In this region the profiles have little structure outside the contact region and the numerical iteration scheme used to solve the Euler–Lagrange equations converges rapidly. Decreasing η_p^r we encounter the point

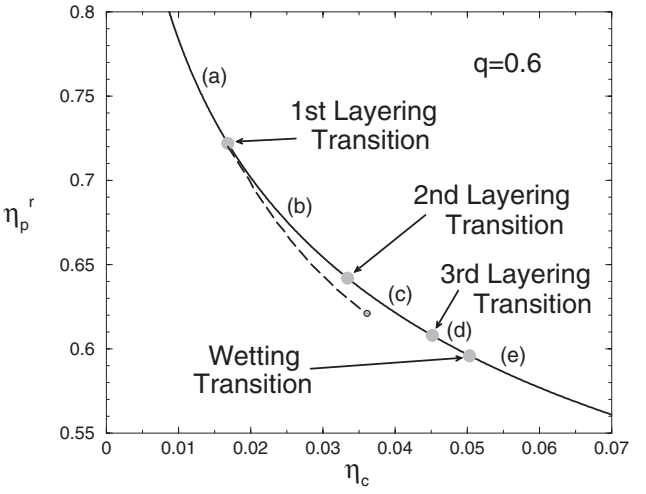

Figure 9. The interfacial phase diagram for a colloid–polymer mixture adsorbed at a hard wall for size ratio $q = 0.6$. The full curve is a portion of the bulk fluid–fluid coexistence curve shown in figure 2. We find a wetting transition at $\eta_{p,\,wet}^r = 0.596$ and three separate layering transitions at higher values of η_p^r. The first layering transition line extends from coexistence to deep into the single phase region (dashed line) and, when crossed, gives rise to a jump in the adsorption as shown in figure 8 for $\eta_p^r = 0.7$; it ends in a surface critical point near $\eta_p^r = 0.62$. The second and third layering transition lines and any prewetting line lie very close to the coexistence curve so the transition lines are simply denoted by circles.

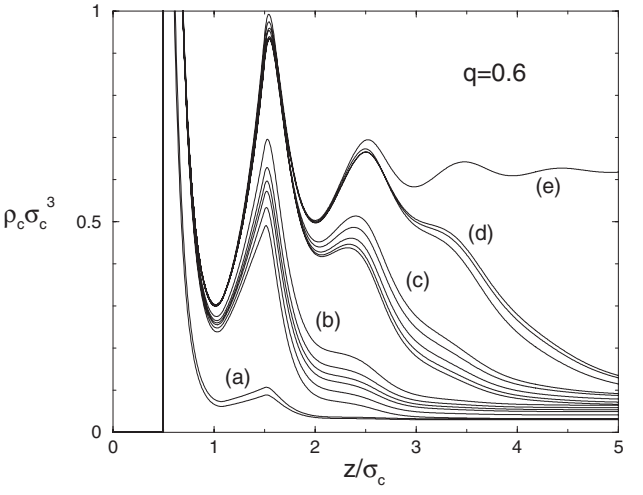

Figure 10. The colloid density profiles calculated at bulk coexistence on decreasing η_p^r (bottom to top) for a size ratio $q = 0.6$. The labels (a)–(e) indicate groups of profiles calculated on the different sections of the coexistence curve, see figure 9, and show clearly the four different transitions, e.g. the higher profile of (a) jumps to the lower profile of (b) at the first layering transition. The first three jumps are layering transitions and the final one, (d) to (e), is the wetting transition. As η_p^r is decreased the adsorption jumps discontinuously as each layering transition is encountered. For $\eta_p^r \lesssim 0.596$ the wall is competely wet by the colloid-rich phase.

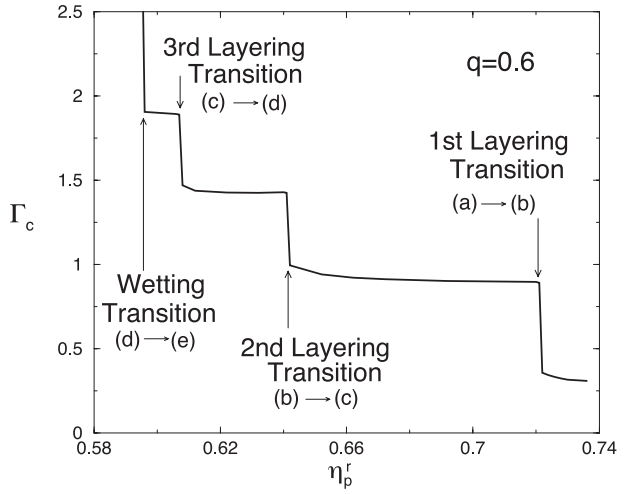

Figure 11. The Gibbs adsorption of the colloids Γ_c along the bulk coexistence curve corresponding to the profiles shown in figure 10, and the phase diagram of figure 9. At each of the layering transitions the adsorption changes discontinuously by a finite amount. At the wetting transition the adsorption diverges discontinuously as the wall is wet completely by the colloid-rich phase.

at which the first layering transition line intersects the phase boundary. Near this point the solution of the Euler–Lagrange equation becomes unstable; this instability is reflected in the number of iterations required to obtain a converged solution. At $\eta_p^r = 0.722$ the adsorption jumps discontinuously and a new layer is adsorbed, see figure 11.

Moving further down the coexistence curve, region (b), the adsorption increases smoothly until a second layering transition occurs at $\eta_p^r = 0.642$, where there is again a discontinuous jump in adsorption as a third layer is adsorbed at the wall. Again the new layer corresponds to a density lower than the coexisting bulk liquid density but it is still liquid-like in character. As the third layer appears the local density in the second layer also jumps significantly, to a value which appears to correspond more closely to that of the coexisting liquid density, i.e. the jump in adsorption at the second transition is only partially due to the appearance of the third layer. Similarly, for $\eta_p^r = 0.608$, we find a third layering transition, (c) to (d), whereby a fourth adsorbed layer develops, with an accompanying increase in density of layer three, giving rise to another jump in Γ_c. As η_p^r is reduced further Γ_c remains finite at bulk coexistence until $\eta_p^r = 0.596$, where the transition to complete wetting occurs. Having located the transition points on the phase boundary, we then take slices at fixed values of η_p^r to determine whether the layering transitions extend into the single phase region. As remarked earlier, the first layering transition extends away from the phase boundary and ends at a surface critical point near $\eta_p^r = 0.62$. In determining the transition line we simply mark the locus of points where the adsorption jumps discontinuously. Such an approach will always be subject to some hysteresis effects, i.e. the actual transition line may be closer to the phase boundary as, for a given η_p^r, we may have to increase η_c above its value at the equilibrium transition in order to move to the next minimum in the free energy. In order to assess the extent of this effect we reversed some of the paths across the phase diagram, starting with a converged solution at coexistence and decreasing η_c until the transition is located. Although hysteresis effects do exist, these are small, and are not visible on the scale of the line in figure 9. Unlike the first transition, the second and third transition lines are extremely short in η_p^r. As it is very difficult to determine these accurately we have simply represented the transitions as large circles in figure 9. The wetting transition appears to be of first order, i.e. Γ_c appears to diverge discontinuously, see figure 11. However, it is difficult to determine any prewetting line, which should emerge tangentially from the coexistence curve at the wetting transition [49]. We can say with certainty that any prewetting line is extremely short. We repeated the calculations for $q = 0.7$ and we find the same pattern of three layering transitions and a wetting transition as was found for $q = 0.6$. The transitions occur at different values of η_p^r, see figure 12. Both the layering transitions and the wetting transition move to larger values of η_p^r on the phase boundary but the distance, in η_p^r, between the first layering transition and the wetting transition remains roughly the same. The first layering transition line is shorter in η_p^r for $q = 0.7$ than for $q = 0.6$ and lies closer to the phase boundary. Figure 13 shows the colloid profiles calculated at bulk coexistence in different regions of the phase diagram, and the corresponding adsorption is shown in figure 14.

For $q = 1$ the distance, in η_p^r, along the bulk phase boundary between the first layering transition and the wetting transition increases and a fourth layering transition appears above the wetting transition—see figure 15. The sequence of colloid density profiles is shown in figure 16. It is interesting to note from figure 17 that at subsequent layering transitions the jump in adsorption is slightly less than that at the preceding one. Since the profiles shown in figure 16 would indicate that the amount adsorbed in each new layer is roughly the same, the difference in adsorption at each transition is due chiefly to the contribution of jumps in the local density at the preceding layer. At the first layering transition the first peak in the colloid profile shows a clear jump, whereas at the fourth transition the local density in the third layer shows little change. We find

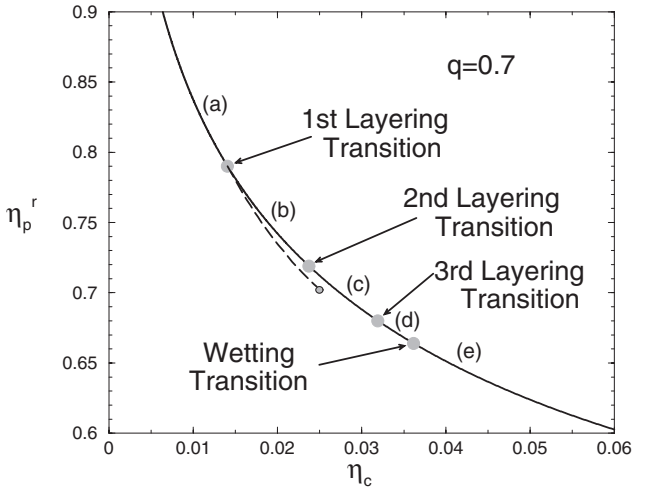

Figure 12. As in figure 9 but for size ratio $q = 0.7$. As for $q = 0.6$, we find three layering transitions but the first layering transition line is slightly shorter in η_p^r and lies closer to the bulk coexistence curve. The wetting transition occurs at $\eta_{p,\,wet}^r = 0.664$.

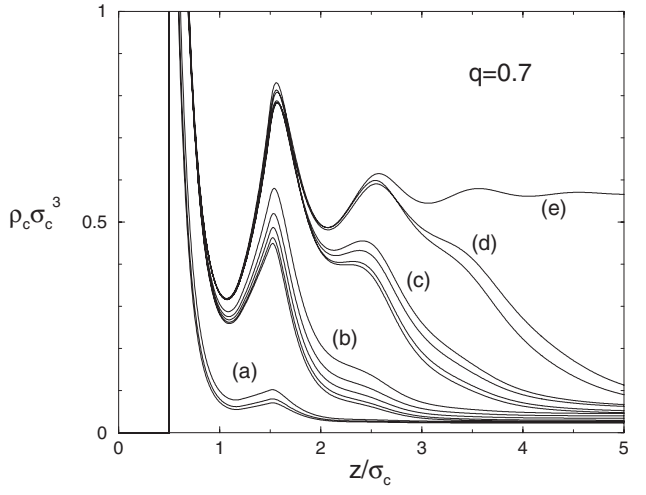

Figure 13. The colloid density profiles at bulk coexistence on decreasing η_p^r (bottom to top) for $q = 0.7$. The labels (a)–(e) indicate groups of profiles calculated on different sections of the coexistence curve, see figure 12.

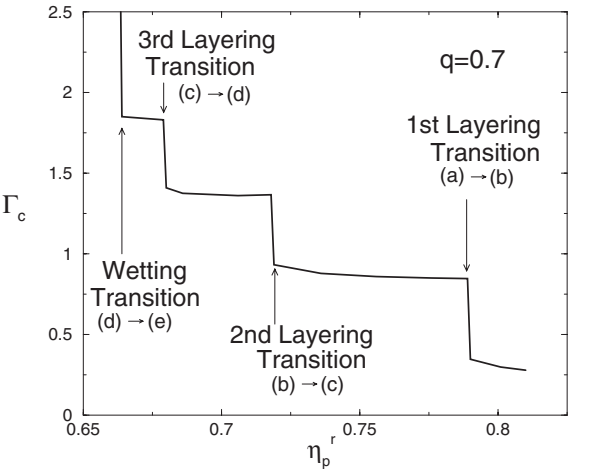

Figure 14. The Gibbs adsorption of the colloids Γ_c along the bulk coexistence curve corresponding to the profiles shown in figure 13 and the phase diagram in figure 12.

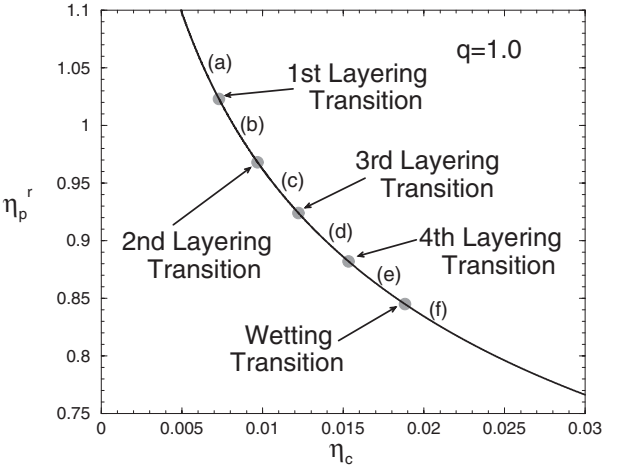

Figure 15. As in figure 9 but for size ratio $q = 1.0$. We find four layering transitions but now all the transition lines, including the first, lie extremely close to the bulk coexistence curve (solid line). The wetting transition occurs near $\eta_{p,\,wet}^r = 0.845$.

that the first layering transition line is very short for $q = 1$ and lies extremely close to the coexistence curve so we simply represent this as a circle in figure 15.

4.3. *A simulation study for* $q = 1$

All the results we have described so far for wetting and layering were based on the DFT for the binary AO mixture. It is important to enquire how much of the rich behaviour predicted by DFT for this model can be found in simulation studies. After the completion of our DFT calculations [25, 26, 46], Dijkstra and van Roij [19] developed a novel Monte Carlo scheme for tackling the equilibrium statistical mechanics of both homogeneous and inhomogeneous model colloid–polymer (AO) mixtures for arbitrary size ratios q, including those where effective many-body interactions between the colloids play an important role. Their approach is based on the exact effective one-component Hamiltonian entering equation (4). Because of the ideality of polymers, $\phi_{pp} = 0$, the grand potential of polymer in the external potential V_p^{ext} and in the static configuration $\{\mathbf{R}^{N_c}\}$ of the N_c colloidal hard spheres is given exactly by $\Omega = -\beta^{-1} z_p V_f$, where

$$V_f = \int d\mathbf{r}\, \exp\left(-\beta V_p^{ext}(\mathbf{r}) \Pi_{i=1}^{N_c} [1 + f_{cp}(|\mathbf{r} - \mathbf{R}_i|)\right] \quad (23)$$

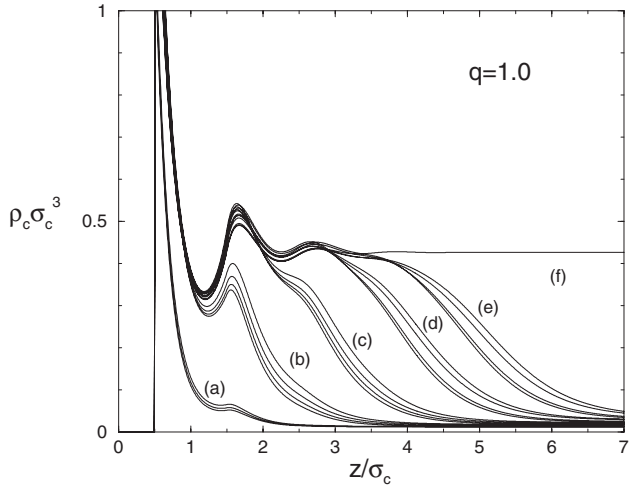

Figure 16. The colloid density profiles at bulk coexistence on decreasing η_p^r (bottom to top) for a size ratio $q = 1.0$. The labels (a)–(f) indicate groups of profiles calculated in different sections of the coexistence curve, see figure 15.

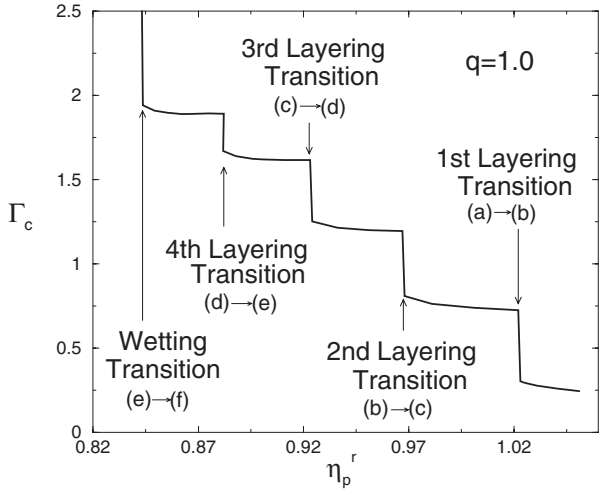

Figure 17. The Gibbs adsorption of the colloids Γ_c along the coexistence curve corresponding to the profiles shown in figure 16 and the phase diagram of figure 15.

is the *free volume*. The integral in equation (23) is over the total volume V of the system and $f_{cp}(r)$ is the colloid–polymer Mayer bond: $f_{cp} = -1$ for $0 < r < R_c + R_p$ and zero otherwise. Of course, the shape of the free volume is, generally, irregular and non-connected but computationally efficient methods were developed to calculate this [19]. Bulk simulations were performed for the case $q = 1$ where effective many-body interactions are expected to be crucially important. The semi-grand free energy was obtained using thermodynamic integration, at fixed colloid packing fraction η_c, with respect to the polymer fugacity z_p (see also [28]).

Phase coexistence was then determined by standard common tangent constructions at fixed z_p. The inset

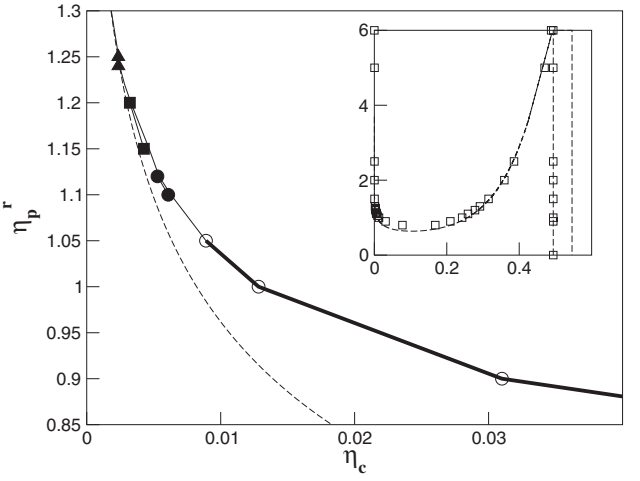

Figure 18. Simulation results (adapted from [19]) for bulk and surface phase diagram of the AO model (size ratio $q = 1$) as a function of the colloid packing fraction η_c and the polymer reservoir packing fraction η_p^r. The main figure is a blow-up of the saturated bulk gas branch, separated into a regime of complete wetting (thick curve, open circles), and partial wetting by colloidal liquid (thin curve) at a planar hard wall. The first (filled triangles), second (filled squares), and third (filled circles) layering transition lines extend from bulk coexistence into the single phase (gas) region. The inset shows the gas–liquid and fluid–solid bulk coexistence (open squares) to full scale. The dashed curves denote the bulk binodals obtained from free-volume theory.

to figure 18 shows the resulting phase diagram in the reservoir, η_p^r versus η_c, representation. Three phases are present; there is colloidal gas–liquid separation, with a critical point $\eta_{p,\,crit}^r \sim 0.70$, and a liquid–solid transition which is almost independent of η_p^r. The triple point is at $\eta_{p,\,t}^r \sim 6.0$, i.e. there is a very large stable gas–liquid coexistence region, much larger than the corresponding (inverse) temperature region for simple atomic fluids. Also plotted in this figure is the phase diagram obtained from the free-volume theory of [4]. Note that the latter can be viewed as a first-order perturbation theory that approximates V_f by its average in the pure hard-sphere fluid [10, 11]; it sets $V_f = \alpha(\rho_c)V$, where $\alpha(\rho_c)$ is the free-volume fraction in equation (16). On the scale of the inset, the free-volume theory, and therefore our DFT approach which yields the same free energy, provides an accurate description of the simulation data. There *are* significant deviations, as indicated on the expanded scale of the main figure where the gas branch of the coexistence curve is plotted, but the overall agreement is quite remarkable. As emphasized by Dijkstra and van Roij [19], it is important to compare the 'exact' simulation phase diagram for $q = 1$ with that obtained in [10] from simulations in which solely the pairwise effective potential $\phi^{eff}(R; z_p)$, equation (6), was employed.

For the latter, $\eta_{p,crit}^{r} \sim 0.5$ and $\eta_{p,t}^{r} \sim 0.8$. In other words, the effective many-body interactions extend greatly the region in η_{p}^{r} over which stable gas–liquid coexistence can occur. Moreover, these many-body contributions appear to be incorporated into the free-volume/DFT approximation. For completeness we should also note that Bolhuis *et al.* [15] have investigated the bulk phase behaviour of the AO binary mixture using Gibbs ensemble Monte Carlo simulations for size ratios $q = 0.34$, 0.67 and 1.05. They find that for $q = 0.34$ the fluid–fluid binodal is (weakly) metastable, consistent with the prediction of the free-volume theory. For $q = 0.67$ and 1.05 their simulation results for the gas–liquid coexistence curves are in good overall agreement with those of the free-volume theory. These authors also performed simulations which incorporate excluded-volume interactions between polymers but we shall return to this aspect later.

The main part of figure 18 displays the surface phase diagram obtained in [19] for the $q = 1$ AO mixture adsorbed at a planar hard wall. Once again V_f (now given by equation (23) with V_p^{ext} corresponding to the hard-wall potential) is calculated within the simulation so that all many-body interactions are incorporated, including the modification of pair and higher-body interactions that occurs when two colloids are close to the wall—see section 2.1 and [11].

For small polymer reservoir packings $\eta_{p,crit}^{r} < \eta_{p}^{r} < 1.05$ there is strong evidence for complete wetting, i.e. formation of a thick film of colloidal liquid at the hard wall–colloidal gas interface with the adsorption Γ_c increasing continuously (logarithmically) as bulk coexistence is approached. In this regime the colloid density profiles (see figure 2(*a*) of [19]) are reminiscent of the DFT results in figure 7. By contrast, for about $\eta_{p}^{r} > 1.1$, there is partial wetting, i.e. Γ_c remains finite at bulk coexistence. The authors conclude that there is a wetting transition at some value of $\eta_{p,wet}^{r}$ in the range $1.05 < \eta_{p,wet}^{r} < 1.1$. They find no evidence for an accompanying prewetting transition out of bulk coexistence, i.e. there appears to be no thin–thick transition in the same range of values of η_{p}^{r}. For about $\eta_{p}^{r} > 1.1$, however, they find jumps in the adsorption which they attribute to layering transitions of the type we found in the DFT calculations described in section 4.2. Indeed the colloid density profiles near the layering transitions (see figure 2(*b*) of [19]) are very similar in form to those shown in figures 10, 13 and 16. Note that the latter refer to transitions encountered on reducing η_{p}^{r} at bulk coexistence, whereas the simulation data is for a path at fixed η_{p}^{r}, increasing η_c towards bulk coexistence. Figure 18 describes three separate layering transition lines, each of them rather short, lying close to bulk coexistence and very far from the bulk triple point. A reasonable person would conclude that the wetting and layering phenomena found in the simulations for $q = 1$ mimic those found in the DFT calculations. There is not perfect agreement. The sequence of layering transitions gleaned from the simulations for $q = 1$, is arguably closer to that observed in DFT for $q = 0.6$ and 0.7 than for $q = 1$; the layering transitions extend very little out of bulk coexistence in the last case (see figure 15). But one should not expect an approximate DFT to provide a completely accurate account of what are very subtle interfacial phase transitions, resulting from a complicated competition between wall–fluid and fluid–fluid interactions. Given that the bulk gas–liquid coexistence curves obtained from DFT and simulation differ significantly on the scale relevant to the surface phase diagram it is not surprising that there are differences in the surface phase behaviour. What is more important is to establish that it is the many-body interactions entering the effective interfacial Hamiltonian for the colloids which give rise to the pattern of interfacial transitions that is observed. We shall return to this issue later.

5. Treating polymer–polymer interactions within a geometry-based DFT

So far in this paper we have treated the polymers as mutually non-interacting: $\phi_{pp}(r) = 0$. Real polymers, when dissolved in a good solvent, experience repulsive monomer–monomer interactions. As described in the introduction, when averaged over polymer conformations this repulsion at the polymer segment level gives rise to a soft, penetrable and repulsive interaction between polymer centres of mass. The range of this effective pair potential is $\gtrsim$ the polymer radius of gyration and its strength (at zero separation between the two centres of mass) is of the order of the thermal energy, $k_B T$. Within this 'soft colloid' picture the effective polymer–polymer potential can be well represented by a Gaussian pair potential [52]. In the following we do not attempt to model this interaction realistically, rather we summarize the approach of [20] where a minimal model was considered that displays the essential features of polymer–polymer repulsion. With a simple geometric picture in mind, the interactions between polymers are represented by a repulsive step-function pair potential

$$\phi_{pp}(r) = \begin{cases} \epsilon, & \text{for } r < 2R_p, \\ 0, & \text{otherwise,} \end{cases} \tag{24}$$

whilst the colloid–colloid and colloid–polymer potentials remain hard-sphere-like. Note that in the limit $\epsilon/k_B T \to 0$ we recover the AO model with non-interacting polymers, equation (1) with $\sigma_p \equiv 2R_p$,

whereas for $\epsilon/k_B T \to \infty$ the model reduces to that of an additive binary hard-sphere mixture. A similar treatment of polymer interactions was introduced by Warren *et al.* [53], although in that work $\phi_{pp}(r)$ was assumed to have a range of R_p, the polymer radius of gyration. Our current (longer-ranged) choice is more consistent with the effective (Gaussian) potentials of Louis *et al.* [52], which extend even beyond $2R_p$. Our aim is to develop a DFT which retains most of the features of the DFT for the original AO model but which incorporates, albeit crudely, polymer–polymer interactions. We briefly review how the DFT of section 2.2 can be extended to the current case, following [20], and then describe the bulk fluid–fluid phase separation which arises in this theory.

5.1. *Construction of the functional*

In constructing functionals for hard-sphere fluids it has been shown [54, 55] that requiring an approximate functional to recover the properties of the system in the zero-dimensional (0d) limit, where the partition sum can be calculated exactly, is a powerful constraint which has guided the development of DFTs for other models, such as the AO model. Thus we first consider the current model in the 0d limit, in which particle centres are confined to a volume v_{0d} whose dimensions are smaller than all relevant length scales in the system. The microstates accessible are then completely specified by the occupation numbers of particles of both species and each microstate is assigned a statistical weight according to the grand ensemble. The grand partition sum for an arbitrary binary mixture in this limit is

$$\Xi = \sum_{N_p=0}^{\infty} \frac{z_p^{N_p}}{N_p!} \sum_{N_c=0}^{\infty} \frac{z_c^{N_c}}{N_c!} \exp(-\beta\phi_{total}), \qquad (25)$$

where the (reduced) fugacities are $z_i = (v_{0d}/\Lambda_i^3) \times \exp(\beta\mu_i)$, Λ_i is the thermal wavelength, μ_i is the chemical potential of species i and ϕ_{total} is the total potential energy in the situation where all particles have vanishing separation. Note that for hard-core interactions, the Boltzmann factor vanishes for forbidden configurations, which then limits the upper bounds in the summations in equation (25). For the present case, where ϕ_{cc} and ϕ_{cp} are hard-body interactions, we obtain

$$\Xi = z_c + \sum_{N_p=0}^{\infty} \frac{z_p^{N_p}}{N_p!} \exp\left(-\beta\epsilon N_p(N_p-1)/2\right), \qquad (26)$$

where the N_p dependence in the Boltzmann factor stems from the counting of pairs of polymers. There are two important limiting cases. For $z_c = 0$ (no colloids), the limit of one-component penetrable spheres [56] is recovered, whereas for $\beta\epsilon = 0$, equation (26) reduces to the AO result [16, 17], $\Xi = z_c + \exp(z_p)$. In order to obtain the Helmholtz free energy, a Legendre transform must be performed, and the dependence on the fugacities replaced with the dependence on the mean (occupation) numbers of particles, $\eta_i = z_i \partial \ln \Xi / \partial z_i$, $i = c, p$. Taking the particle volume of species i as the reference volume, η_i is also the 0d packing fraction of species i. Subtracting the ideal contribution, one calculates the excess Helmholtz free energy, $\beta F_{0d} = -\ln \Xi + \sum_{i=c,p} \eta_i \ln(z_i) - \sum_{i=c,p} \eta_i [\ln(\eta_i) - 1]$. In the present case (as for pure penetrable spheres [56]), this cannot be expressed analytically. As we are interested in the case of small ϵ (small deviations from the AO model), we perform an expansion in powers of $\beta\epsilon$, and obtain

$$\beta F_{0d}^{(1)} = (1-\eta_c-\eta_p)\ln(1-\eta_c) + \eta_c + \frac{\beta\epsilon}{2}\frac{{\eta_p}^2}{1-\eta_c}, \qquad (27)$$

which is exact up to lowest (linear) order in $\beta\epsilon$. In the limit $\beta\epsilon \to 0$, equation (27) reduces to the AO result [16, 17], which is $\beta F_{0d,AO} = (1-\eta_c-\eta_p)\ln(1-\eta_c) + \eta_c$. In the absence of colloids, $\eta_c \to 0$, we obtain a mean-field-like expression, $F_{0d,MF} = \epsilon {\eta_p}^2/2$.

Since some terms of higher than first order can be obtained analytically, we write the free energy as $F_{0d}^{(1)} + \Delta F_{0d}$, and we find that up to cubic order in $\beta\epsilon$

$$\beta\Delta F_{0d} = -\frac{{\eta_p}^2(\beta\epsilon)^2}{4(1-\eta_c)} + \left[\frac{{\eta_p}^2}{1-\eta_c} + \frac{2{\eta_p}^3}{(1-\eta_c)^2}\right]\frac{(\beta\epsilon)^3}{12}. \qquad (28)$$

For large $\beta\epsilon$, the 0d free energy must be calculated numerically. This is straightforward [20].

Returning to three dimensions, we write the excess Helmholtz free energy functional of an inhomogeneous system as

$$\beta\mathcal{F}_{ex}[\rho_c(\mathbf{r}), \rho_p(\mathbf{r})] = \int d\mathbf{r}\, \Phi\left(\{n_\nu^c\}, \{n_\gamma^p\}\right), \qquad (29)$$

which is the same as in the ideal polymer case, equation (11). The weighted densities $\{n_\nu^i\}$ are defined as convolutions with the bare density profiles through equation (13). In addition to the weights (14) we also introduce Tarazona's [57] tensor weight function $\hat{\mathbf{w}}_{m2}^i(\mathbf{r}) = w_2^i(\mathbf{r})[\mathbf{rr}/r^2 - \hat{\mathbf{1}}/3]$, where $\hat{\mathbf{1}}$ is the identity matrix.

The free energy density is composed of three parts

$$\Phi = \Phi_1 + \Phi_2 + \Phi_3\,, \qquad (30)$$

which are defined as

$$\Phi_1 = \sum_{i=\mathrm{c,p}} n_i^0 \varphi_i\left(n_3^{\mathrm{c}}, n_3^{\mathrm{p}}\right), \tag{31}$$

$$\Phi_2 = \sum_{i,j=\mathrm{c,p}} \left(n_1^i n_2^j - \mathbf{n}_{\mathrm{v}1}^i \cdot \mathbf{n}_{\mathrm{v}2}^j\right)\varphi_{ij}\left(n_3^{\mathrm{c}}, n_3^{\mathrm{p}}\right), \tag{32}$$

$$\Phi_3 = \frac{1}{8\pi} \sum_{i,j,k=\mathrm{c,p}} \left(\frac{1}{3} n_2^i n_2^j n_2^k - n_2^i \mathbf{n}_{\mathrm{v}2}^j \cdot \mathbf{n}_{\mathrm{v}2}^k + \frac{3}{2}\left[\mathbf{n}_{\mathrm{v}2}^i \mathbf{n}_{\mathrm{m}2}^j \mathbf{n}_{\mathrm{v}2}^k - \mathrm{tr}\left(\mathbf{n}_{\mathrm{m}2}^i \mathbf{n}_{\mathrm{m}2}^j \mathbf{n}_{\mathrm{m}2}^k\right)\right]\right)\varphi_{ijk}\left(n_3^{\mathrm{c}}, n_3^{\mathrm{p}}\right), \tag{33}$$

where tr denotes the trace. The quantities φ_i, φ_{ij} etc. are derivatives of the 0d excess free energy

$$\varphi_{i\ldots k}(\eta_{\mathrm{c}}, \eta_{\mathrm{p}}) \equiv \frac{\partial^m}{\partial\eta_i \ldots \partial\eta_k} \beta F_{0\mathrm{d}}(\eta_{\mathrm{c}}, \eta_{\mathrm{p}}). \tag{34}$$

In the absence of polymer, Φ_1 and Φ_2 are equivalent to the free energy densities for hard spheres introduced in [18] and Φ_3 is equivalent to the tensor treatment for pure hard spheres in [57]. Equations (31)–(33) are generalizations of these earlier treatments that include summations over species. If we set $\beta\epsilon = 0$, ideal polymer, and take the derivatives of $\beta F_{0\mathrm{d,AO}}$ we recover the explicit expressions given in equation (12) for the AO model.

5.2. *Fluid–fluid phase separation*

In bulk, the one-body densities of both species are spatially uniform: $\rho_i(\mathbf{r}) = \mathrm{const}$. This leads to simple analytic expressions for the weighted densities. The excess free energy density, equations (30)–(33), is easily evaluated provided the analytic approximations (27), (28) are employed for $F_{0\mathrm{d}}$. If we retain only the linear term in $\beta\epsilon$, i.e. employ equation (27), then

$$\beta f_{\mathrm{ex}}(\rho_{\mathrm{c}}, \rho_{\mathrm{p}}) = \frac{\beta\mathcal{F}_{\mathrm{ex}}(\rho_{\mathrm{c}}, \rho_{\mathrm{p}})}{V} = \beta f_{\mathrm{ex}}^{\mathrm{HS}}(\rho_{\mathrm{c}}) - \rho_{\mathrm{p}} \ln \alpha_1(\rho_{\mathrm{c}}) + \frac{\beta\tilde{\phi}_{\mathrm{pp}}(0)}{2}\rho_{\mathrm{p}}{}^2[1 - \ln\alpha_2(\rho_{\mathrm{c}})], \tag{35}$$

where the integrated potential is $\tilde{\phi}_{\mathrm{pp}}(0) = 4\pi\int \mathrm{d}r\, r^2\phi_{\mathrm{pp}}(r) = 4\pi\epsilon\sigma_{\mathrm{p}}^3/3$. $f_{\mathrm{ex}}^{\mathrm{HS}}$ is the scaled-particle (Percus-Yevick compressibility) approximation, and is given by

$$\beta f_{\mathrm{ex}}^{\mathrm{HS}} = \frac{3\eta_{\mathrm{c}}[3\eta_{\mathrm{c}}(2-\eta_{\mathrm{c}}) - 2(1-\eta_{\mathrm{c}})^2 \ln(1-\eta_{\mathrm{c}})]}{8\pi R_{\mathrm{c}}^3(1-\eta_{\mathrm{c}})^2}, \tag{36}$$

and is the same quantity that enters equation (15). The quantities α_1 and α_2, which depend solely on η_{c} and the size ratio $q = \sigma_{\mathrm{p}}/\sigma_{\mathrm{c}}$, are given by

$$\ln\alpha_1 = \ln(1-\eta_{\mathrm{c}}) - \sum_{m=1}^{3} C_m^{(1)}\gamma^m, \tag{37}$$

$$\ln\alpha_2 = -\frac{1}{8}\sum_{m=1}^{4} C_m^{(2)}\gamma^m, \tag{38}$$

where the dependence on colloid density is through $\gamma = \eta_{\mathrm{c}}/(1-\eta_{\mathrm{c}})$, and the coefficients are polynomials in the size ratio, given as $C_1^{(1)} = 3q + 3q^2 + q^3$, $C_2^{(1)} = (9q^2/2) + 3q^3$, $C_3^{(1)} = 3q^3$ and $C_1^{(2)} = 8 + 15q + 6q^2 + q^3$, $C_2^{(2)} = 15q + 24q^2 + 7q^3$, $C_3^{(2)} = 18q^2 + 15q^3$ and $C_4^{(2)} = 9q^3$.

For $\beta\epsilon = 0$, ideal polymer, our result is identical to that of free-volume theory for the AO model—see equations (15) and (16). The quantity α_1 in equation (37) is identical to α, the free-volume fraction of a single polymer sphere in the AO model. α_2 can be interpreted [20] as the free-volume ratio for pairs of overlapping polymers. α_1 and α_2 both decrease monotonically with increasing η_{c} due to the increasing excluded volume. However, $\alpha_2 > \alpha_1$ over the whole density range, which may be due to correlations between polymer pairs [20]. At fixed η_{c}, both α_1 and α_2 decrease monotonically with increasing size ratio.

The total canonical free energy is given by $F/V = f_{\mathrm{ex}} + k_{\mathrm{B}}T\sum_{i=\mathrm{c,p}}\rho_i[\ln(\rho_i\Lambda_i^3) - 1]$. It is convenient to transform to the semi-grand ensemble, where the polymer chemical potential μ_{p} is prescribed instead of the system density ρ_{p}. The appropriate thermodynamic potential is the semi-grand free energy Ω_{semi}, related to F via a Legendre transform: $\Omega_{\mathrm{semi}}/V = F/V - \mu_{\mathrm{p}}\rho_{\mathrm{p}}$, where μ_{p} is given as

$$\beta\mu_{\mathrm{p}} = \partial(\beta F/V)/\partial\rho_{\mathrm{p}} = \ln(\rho_{\mathrm{p}}\Lambda_{\mathrm{p}}^3) - \ln\alpha_1(\rho_{\mathrm{c}}) - \beta\tilde{\phi}_{\mathrm{pp}}(0)\rho_{\mathrm{p}}[1 - \ln\alpha_2(\rho_{\mathrm{c}})], \tag{39}$$

which is a transcendental equation to be solved for ρ_{p} once μ_{p} is prescribed. This result is a generalization of the standard free-volume expression $\beta\mu_{\mathrm{p}} = \ln(\Lambda_{\mathrm{p}}^3\rho_{\mathrm{p}}/\alpha)$ pertaining to the original AO model [4].

As usual, phase coexistence is determined by requiring equality of the total pressure, of the chemical potentials μ_i, and of the temperatures in the coexisting phases. This can be carried out in the system representation $(\eta_{\mathrm{c}}, \eta_{\mathrm{p}})$ [20] or, using common tangent constructions on Ω_{semi}, in the polymer reservoir representation $(\eta_{\mathrm{c}}, \mu_{\mathrm{p}})$.

Stable fluid–fluid phase separation (with respect to the fluid–solid transition) is observed in experiments

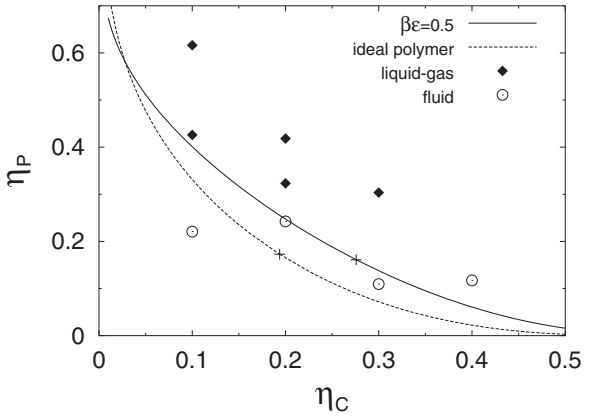

Figure 19. Fluid demixing binodals in the system representation, i.e. as a function of the colloid (η_c) and polymer (η_p) packing fractions for size ratio $q = 0.57$. Results are shown for the case of non-interacting polymer (dashed line) and for interacting polymer (solid line) with strength $\beta\epsilon = 0.5$. The crosses denote the critical points. The symbols refer to the experimental state points taken from [5]. The open circles denote single-phase (fluid) states and the filled rhombuses two-phase (liquid–gas) states.

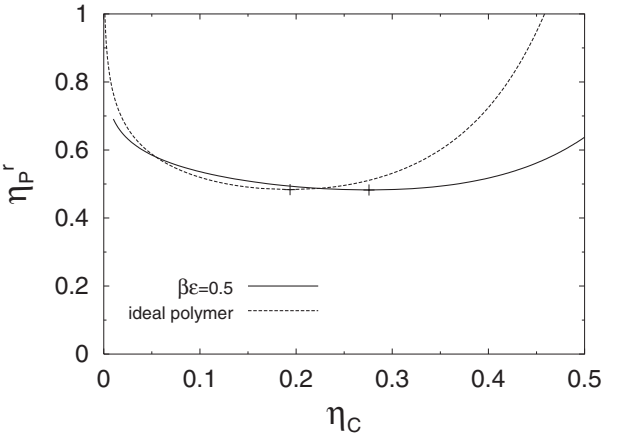

Figure 20. Same as figure 19 ($q = 0.57$), but in the reservoir representation, i.e. as a function of η_c and the packing fraction of polymer (η_p^r) in a reservoir of pure polymer in osmotic equilibrium with the system.

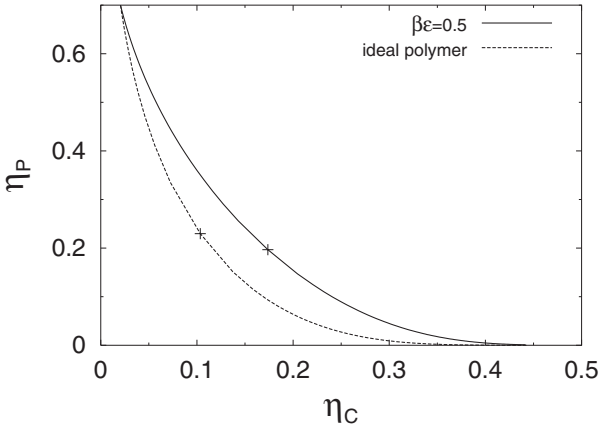

Figure 21. Same as figure 19, but for size ratio $q = 1$.

on colloid–polymer mixtures only at sufficiently large polymer-to-colloid size ratios. We consider the size ratio $q = 0.57$, for which experimental data are available for PMMA colloid and polystyrene (PS) in *cis*-decalin [5]. Figure 19 shows the calculated phase diagrams with and without polymer interactions. For non-interacting polymers ($\beta\epsilon = 0$), our result is identical to that from free volume theory for the AO model. In order to apply our theory to the experimental situation, we have prescribed the potential energy barrier to be $\beta\epsilon = 0.5$. This is based on considerations of the second virial coefficient of a pure polymer solution [20]. In order to achieve higher accuracy than is provided by the linear expansion of the 0d free energy, equation (27), we use the cubic order expression, equation (28), to determine the excess free energy. Figure 19 shows a comparison of the calculated theoretical binodal with the experimental data of [5] in the system representation.

Although the measured single-phase (fluid) state point at high colloid packing fraction lies inside the theoretical two-phase region, it is clear that our theory predicts a shift in the correct direction compared with the non-interacting (ideal) binodal. The theory also predicts that the coexisting colloidal gas phase is more strongly dilute in colloids, as compared with the non-interacting case.

In figure 20 the phase diagram is shown in polymer reservoir representation: a reservoir of *interacting* pure polymer is considered that is in chemical (osmotic) equilibrium with the system with respect to exchange of polymers. The tie lines are horizontal in this representation. Away from the critical point a gas, dilute in colloids, coexists with a liquid that has very high packing fraction of colloids, much higher than in the ideal case. We consider next the case of equally-sized species, $q = 1$. Phase diagrams are shown in the system representation (figure 21) and in the reservoir representation (figure 22). Again a marked shift of the critical point towards higher η_c is found and the single phase region is larger (in the system representation) compared to the case of ideal polymer. Figure 22 shows that the packing fraction of coexisting liquid increases quite rapidly with increasing η_p^r, which has repercussions for the location of the triple point. All these results can be understood in terms of a free energy penalty arising from polymer–polymer interactions. These manifest themselves primarily in the colloidal gas phase as only a small penalty arises in the colloidal liquid phase, where polymers are strongly diluted.

It is instructive to make some comparisons between the present results and the recent extensive Monte Carlo simulation results of Bolhuis *et al.* [15] mentioned in

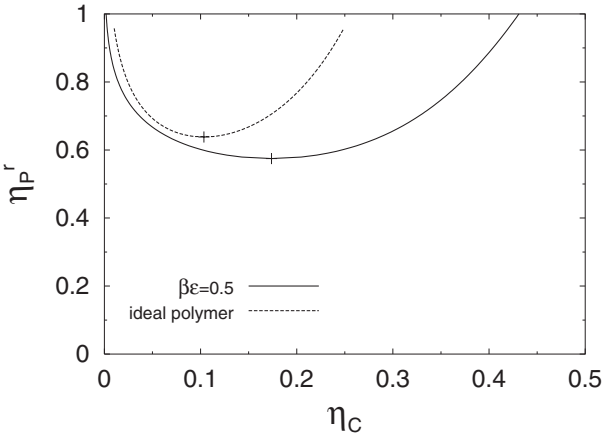

Figure 22. Same as figure 20, but for size ratio $q = 1$.

section 4.3. These authors consider hard-sphere colloids but obtain effective potentials for the polymer–polymer interaction from simulations of a bulk system of self-avoiding walks (SAW) at various concentrations—a procedure known to be reliable for polymers in a good solvent. The effective pair potentials ϕ_{pp} correspond to tracing out the monomer degrees of freedom and treating the polymer as 'soft colloid'; ϕ_{pp} depends on the volume fraction of the polymer and is calculated by inversion of the centre-of-mass radial distribution function $g_{pp}(r)$. The colloid–polymer effective potential also depends on the volume fraction of polymer. It is obtained from simulations of a single hard sphere in a solution of SAW polymers by inverting the centre-of-mass concentration profile using the HNC equation—details are given in [15]. Phase diagrams are determined by Gibbs ensemble simulations of the binary mixture described by these effective pair potentials and results are presented for $q = 0.34$, 0.67 and 1.05. We focus here on size ratios $q = 0.67$ and 1.05 where gas–liquid (fluid–fluid) phase separation is stable with respect to fluid–solid.

In the (η_c, η_p^r) representation including polymer–polymer interactions increases the critical point value of the packing fraction of colloids very slightly but increases the critical polymer reservoir fraction $\eta_{p,\,crit}^r$ by about 0.25 for $q = 0.67$. More significantly, the gas–liquid two-phase region is broadened significantly in η_c and the triple point $\eta_{p,\,t}^r$ is lowered considerably from what is found in the ideal polymer (AO) case—see figure 1 of [15]. The upshot is that there is a very narrow, in η_p^r, region of stable fluid–fluid phase coexistence when interactions are included. This is not totally different from what we find in figure 20, for $q = 0.57$, from the DFT; as freezing is expected to occur when $\eta_c \sim 0.5$, this permits only a small separation between $\eta_{p,\,t}^r$ and $\eta_{p,\,crit}^r$ when interactions are incorporated. However, our DFT does not predict the substantial increase in $\eta_{p,\,crit}^r$ which is found in simulations when interactions are included. This is reflected clearly in the (η_c, η_p) representation where the binodal calculated with interactions appears to be more separated from the non-interacting case (see figure 2 of [15]) giving a larger single-phase region than in the corresponding DFT results, although the latter are for a smaller value of q. The situation is exaggerated for $q = 1.05$. Now the critical point is shifted from $\eta_{c,\,crit} \sim 0.11$, $\eta_{p,\,crit}^r \sim 0.75$ to $\eta_{c,\,crit} \sim 0.18$, $\eta_{p,\,crit}^r \sim 1.12$ and the triple point is lowered from what is a very high number $\eta_{p,\,t}^r \sim 6$ to $\eta_{p,\,t}^r \sim 1.65$ when interactions are included. Again the range in η_p^r over which stable fluid–fluid phase coexistence occurs is narrowed considerably. A similar trend is found in the DFT results of figure 22 for $q = 1$ but the latter predict a small *decrease* in $\eta_{p,\,crit}^r$ rather than the substantial increase found in simulation. Moreover, the DFT does not predict the very strong shift of the binodal in the (η_c, η_p) representation found in simulations (figure 3 of [15]) which results in a much larger single-phase region when interactions are included.

In summary, the DFT introduced in [20] and described above captures several, but not all, of the effects of polymer–polymer excluded volume interactions that are found in the computer simulations of bulk phase behaviour. (Note, however, that the freezing transition was not considered explicitly in the DFT calculations.) This should encourage applications of the theory to *inhomogeneous* situations—the primary purpose of DFT. Such problems are not easily tackled by simulations.

Of course, this model of polymer–polymer interactions is highly idealized and a detailed critique is given in [20]. The main limitations are: (i) $\phi_{pp}(r)$ is assumed to be a step function rather than a Gaussian-type function, (ii) the range of the step function is set equal to $2R_p$, twice the polymer radius of gyration, in order to derive a geometry-based DFT meeting 'additive' restrictions and (iii) the strength ϵ and range of ϕ_{pp} are assumed to be independent of the concentrations of polymer and colloids, whereas simulation studies of SAW [15, 52] indicate that the effective polymer–polymer potential should depend on the volume fraction of polymer.

We conclude this section by emphasizing [20] that the present DFT approach is *not* a perturbative treatment of polymer–polymer interactions. One might attempt to construct a DFT which starts with the AO functional for the AO reference model and then simply adds a (perturbative) contribution to account for polymer–polymer interactions. The latter could be the type of mean-field functional used recently to describe a pure polymer system [21], namely

$$\mathcal{F}_{MF}[\rho_p(\mathbf{r})] = \frac{1}{2}\int d\mathbf{r} \int d\mathbf{r}' \rho_p(\mathbf{r})\rho_p(\mathbf{r}')\phi_{pp}(|\mathbf{r} - \mathbf{r}'|). \quad (40)$$

This functional generates the pair direct correlation function which corresponds to the random phase approximation: $c_{pp}^{(2)}(\mathbf{r},\mathbf{r}') = c_{pp}^{(2)}(|\mathbf{r}-\mathbf{r}'|) = -\beta\phi_{pp}(|\mathbf{r}-\mathbf{r}'|)$, known to be a good approximation at high densities for penetrable potentials [21]. It has been used to good effect in investigations of repulsive Gaussian core particles adsorbed at a hard wall [58]. The generalization of equation (40) to binary Gaussian core mixtures was used in studies of fluid–fluid interfaces [41] and of wetting phenomena [48]. At first sight the functional $\mathcal{F}_{ex}^{AO} + \mathcal{F}_{MF}$ would appear to provide a reasonable description of the excess free energy of the AO mixture; note that the hard-body interactions between colloids and polymers are already included in $\mathcal{F}_{ex}^{AO}$. However, as shown in [20], this is *not* the case for the model described above. The perturbative contribution $\mathcal{F}_{MF}$ depends solely on the polymer density $\rho_p(\mathbf{r})$ and therefore neglects exclusion of polymer from the volume occupied by the colloids. By contrast the geometry-based DFT builds in excluded volume effects. One can understand this by returning to the 0d free energy, equation (27). The final (polymer) contribution is enhanced over the corresponding mean-field expression $\beta\epsilon\eta_p^2/2$ by a factor $(1-\eta_c)^{-1}$. The perturbative DFT exhibits some severe failings when applied to the calculation of phase behaviour and similar failings are to be expected [20] if the same approach, i.e. simply adding $\mathcal{F}_{MF}$ to $\mathcal{F}_{ex}^{AO}$, were adopted for other models, e.g. mixtures of hard-core and Gaussian particles. Note that the approach of Warren *et al.* [53] for the bulk free energy can be viewed as a perturbative treatment in which $\phi_{pp}(r)$ is regarded as a perturbation about the AO reference system. Schmidt *et al.* [20] rederive the theory of [53] in a framework that allows them to understand relationships between the various approaches. They argue that the geometry-based DFT provides a more realistic account of the binodal than does the theory of [53].

6. Further developments

During the last two years several applications and extensions of the DFT for the AO model have been reported. We summarize some of them in this section. An overview of geometry-based DFT, which lists a wider range of developments, is given by Schmidt [59].

We mention first two direct applications of the DFT for the AO mixture described in section 2.2. As a planar hard wall prefers the colloid-rich (liquid) phase to the colloid-poor (gas) phase, the hard wall–liquid surface tension is lower than the hard wall–gas tension. General arguments [60] then imply that for the colloid–polymer mixture confined between two, parallel, planar hard walls, capillary condensation of the liquid phase should occur when the reservoir fluid is in the gas phase, i.e. for a given η_p^r the value of μ_c is lower than the bulk coexistence value. Brader observed this phenomenon in his PhD studies [25] using the DFT. Systematic investigations were carried out recently [61] using both DFT and computer simulation. Lines of capillary condensation were determined for size ratio $q = 1$. These are most easily represented in the (μ_c, η_p^r) plane, where μ_c is the colloid chemical potential. Upon decreasing the (scaled) wall separation distance H/σ_c from ten to two a pronounced shift of the capillary binodal towards smaller values of μ_c occurs. The critical point shifts to larger η_p^r, corresponding to lower temperature in the case of a simple atomic fluid, *and* to larger μ_c upon reducing H. This latter trend seems to be much more pronounced in the simulation results than in those from DFT. Preliminary investigations demonstrated that the shift of the binodal could be described reasonably well using the generalized (to binary mixtures) Kelvin equation for capillary condensation [62]. The practical importance of this investigation lies in possible experimental realizations by strongly confining (between glass substrates) real colloid–polymer mixtures [63]. From a theoretical viewpoint one sees that since all the bare interactions in this system are either hard or ideal, this is an important example of shifting a bulk phase transition, via confinement, by means of purely entropic (depletion) forces.

The second application refers to the AO model colloid–polymer mixture exposed to a standing laser field that is modelled as an external potential acting on the colloids. This has a sinusoidal variation as a function of the space coordinate in the direction of the beam [64]. DFT results indicate that the external potential may stabilize a 'stacked' fluid phase which is a periodic succession of liquid and gas slabs. The regions of large laser intensity (where the external potential is small) are filled with colloidal liquid whereas the regions with small laser intensity are gas-like.

Several extensions of the AO model have been made and the bulk phase behaviour compared with the original. In order to take into account the effect of poor solvent quality on colloid–polymer mixtures, the solvent was modelled as a distinct component. Specifically it was taken to be a binary mixture of a primary solvent that is treated (as usual) as a homogeneous, inert background and a secondary cosolvent that is treated as an ideal gas of point particles [65]. These cosolvent particles are assumed to penetrate neither the polymers nor the colloids. In the absence of colloids, the polymer–cosolvent subsystem is the Widom–Rowlinson model [66] of a binary mixture in which particles of like species are non-interacting while unlike species interact with hard cores. Thus the cosolvent induces an effective many-body attraction between the polymers, reminiscent of that caused by poor solvent.

It was found that worsening the solvent quality, by increasing the cosolvent concentration, increases greatly the tendency to demix, i.e. this shifts the corresponding binodal to smaller colloid and polymer packing fractions [65].

The shape and size of real polymers will be affected by confinement effects, generated by the presence of the colloidal particles in a colloid–polymer mixture. In order to model the effect on the polymer size distribution, an AO model with polydisperse polymer spheres was considered [67]. The polymer spheres are mutually non-interacting but are excluded from the colloids; their radii are free to adjust to allow for colloid-induced compression. The size (radius of gyration) probability distribution in the polymer reservoir was taken to be that of ideal chains. It was found that the presence of the colloids reduces considerably the average polymer size. As a consequence, the bulk demixing binodal is shifted towards higher polymer densities, stabilizing the single, mixed phase as compared with the incompressible AO case.

For very large polymer-to-colloid size ratios the assumption that colloids cannot penetrate polymers is no longer valid. A small colloidal sphere may well penetrate the open coil structure of a big polymer. In order to incorporate this effect on the level of an effective sphere model a penetrable AO model was introduced [68]. The colloid–polymer interaction is assumed to be a step-function of *finite* height, in contrast to the hard-core repulsion of the conventional AO case. The range of this interaction is still taken to be $R_c + R_p$, and the strength is taken from the known immersion free energy of a single sphere in a dilute solution of polymer coils or in a theta solvent. The colloid–colloid interaction remains hard-sphere-like and $\phi_{pp} = 0$. For large size ratios, $q \gtrsim 3$, there is a significant increase in the extent of the mixed region in the phase diagram compared to the free-volume result for impenetrable polymer, i.e. for the AO model [68]. These findings are in keeping with results from more microscopic approaches which treat excluded volume at the segment level [14].

A system that is closely related to the AO model is a mixture of spherical hard-sphere colloids and hard, needle-like particles. The latter may represent either stretched polymers or stiff colloidal rods. In the simplest model [69] the thickness of the rods is set to zero such that rod–rod interactions can be ignored but there remains an excluded volume interaction between a rod and a hard sphere. For this model there is no liquid crystalline order, because of the absence of rod–rod interactions. However, simulation studies found isotropic gas and liquid phases as well as a solid phase [69]. The rods act as a depletant, in a similar fashion to the non-interacting polymer spheres in the AO model, and give rise to an effective attraction between the hard-sphere colloids. Bolhuis and Frenkel [69] also determined the phase behaviour using a free-volume approximation for the free energy, similar to that of Lekkerkerker *et al*. [4] for the AO model, i.e. a first-order perturbation theory that sets the free-volume fraction for the needles equal to its average value in the pure hard-sphere fluid. A DFT was constructed [22] for this model and applied subsequently [23] to the planar (free) interface between demixed fluid phases, one of which, the liquid, is rich in spheres (and poor in needles) and the other, the gas, is dilute in spheres (and rich in needles). Note that in constructing the DFT it was necessary to introduce a weight function $w_2^{SN}(\mathbf{r}, \mathbf{\Omega})$, where $\mathbf{\Omega}$ refers to the orientation of the needles, which contains information about both species, the spheres and the needles, in order to generate the sphere-needle Mayer bond. The corresponding sphere-needle weighted density, $n_2^{SN}(\mathbf{r}, \mathbf{\Omega})$, is a convolution of the sphere density $\rho_s(\mathbf{r})$ and $w_2^{SN}(\mathbf{r}, \mathbf{\Omega})$, whereas all the remaining weighted densities involve only variables of an individual species. For uniform fluids the DFT yields the following expression for the excess free energy density:

$$\beta f_{ex}(\rho_S, \rho_N) = \beta f_{ex}^{HS}(\rho_S) - \rho_N \ln \alpha(\rho_S), \qquad (41)$$

where ρ_S and ρ_N refer to the number densities of spheres and needles, respectively. f_{ex}^{HS} is, as usual, the excess free energy density of pure hard spheres (36) and $\alpha(\rho_S)$ is the free-volume fraction for a single, test needle of length L in the hard-sphere fluid:

$$\alpha(\rho_S) = (1 - \eta) \exp[-(3/2)(L/\sigma)\eta/(1 - \eta)], \qquad (42)$$

with $\eta = \pi\rho_S\sigma^3/6$, the packing fraction of spheres of diameter σ. Equation (41) is identical to the free-volume result [69] and can also be obtained by applying scaled-particle theory for non-spherical bodies [70] to the current model. It has the same form as the excess free energy for the AO model—see equation (15). The fluid–fluid binodal resulting from equation (41) was found to be rather close to that obtained by simulations for the case $L/\sigma = 1$ [69]. Brader *et al*. [23] chose the same size ratio for their DFT studies of the planar fluid–fluid interface. The bulk phase diagram, plotted in the reservoir representation, i.e. $\rho_*^r = \rho_N^r L^2\sigma$ versus η, has a similar form to figure 2 with $\eta = \eta_c$ and ρ_*^r, the reduced needle density in the reservoir, replacing the polymer reservoir packing fraction η_p^r. The critical point is located at $\eta_{crit} = 0.158$ and $\rho_{*,\,crit}^r = 14.64$ whilst the triple point, estimated from first-order perturbation theory [69], is at $\rho_{*,\,t}^r = 24$. As in figure 2, there is a Fisher–Widom (FW) line intersecting the liquid branch of the binodal near $\rho_{*,\,FW}^r = 17$, see figure 2 of [23]. For coexisting states with higher values of ρ_*^r, on the

oscillatory side of the FW line, Brader *et al.* find sphere density profiles $\rho_S(z)$ that are oscillatory on the sphere-rich (liquid) side of the planar interface. However, the amplitude of the oscillations is considerably smaller than what was described in section 3 for the AO model. As expected, on the needle-rich (gas) side the density profile of the spheres decays monotonically into bulk for all states. The important new feature which arises in this study concerns the nature of the needle density profiles. Within DFT one can determine the one-body density $\rho_N(z,\theta)$, where z is the perpendicular distance from the interface and θ is the angle between the needle orientation and the interface normal, and hence both the orientation averaged needle density profile, $\bar{\rho}_N(z)$, and the orientational order parameter profile $\langle P_2(\cos\theta)\rangle$. For states above the FW line, $\bar{\rho}_N(z)$ displays very weak oscillations on the liquid side of the interface arising from the influence of the packing of the spheres on the distribution of the needles. From the result for $\langle P_2(\cos\theta)\rangle$, Brader *et al.* conclude that needles order parallel to the interface on the needle-rich side. This appears to be similar to the biaxial ordering of needles that occurs at a planar hard wall; in the present case the densely packed hard-sphere fluid acts as a 'wall' for the needles. On the sphere-rich side the needles prefer to orient themselves perpendicular to the interface and this is interpreted as the needles protruding through the voids in the first layers of the hard-sphere fluid. These general features of the orientational order are independent of the size ratio L/σ. As an optimal compromise between manageable needle particle numbers and simulation box size, Bolhuis *et al.* [71] chose to perform Monte Carlo simulations with ratio $L/\sigma = 3$. The different preferential alignment of needles on either side of the interface is confirmed by the simulation results. Moreover, there is remarkable quantitative agreement between simulation and DFT results for the density profiles $\rho_S(z), \bar{\rho}_N(z)$ and the orientational order parameter profile [71]. Brader *et al.* [23] also describe results for the liquid–gas surface tension and discuss what might be appropriate scaling factors to bring about data collapse for different size ratios L/σ.

In a related study Roth *et al.* [24] considered the same sphere–needle mixture, with $L/\sigma = 1$, adsorbed at a planar hard wall—the same type of situation as that described in section 4. Density profiles calculated from the DFT for the binary mixture of spheres and needles show that complete wetting of the hard wall–gas interface by the sphere-rich, liquid phase occurs upon approaching the binodal on a path at fixed $\rho_*^r = 16$; the profiles are reminiscent of those in figure 7. There appears to be complete wetting for all the values of ρ_*^r considered. An effective one-component description of the same system was also investigated in [24]. This follows the approach of section 2.1 in that a sphere–sphere and a wall–sphere depletion potential can be obtained by integrating out the degrees of freedom of the needles (rods) [72]. Since the needles are mutually non-interacting the depletion potentials depend linearly on ρ_N^r. Geometrical arguments, similar to those for the AO model, show that the effective one-component Hamiltonian corresponding to equation (9) should be exact for $L/\sigma < 1 - (2(3^{1/2}) - 3)^{1/2} = 0.31875$, which should be compared with the corresponding size ratio $q = \sigma_p/\sigma_c = 0.1547$ for the AO model. Thus, for the system under consideration, with $L/\sigma = 1$, there are many-body effective interactions which are not included in the analogue of equation (9). Ignoring these, Roth *et al.* [24] employed a one-component DFT, equivalent to that used in [11] for adsorption studies of the AO model with $q = 0.1$; this treats the hard-sphere contribution by the Rosenfeld FMT and the depletion attraction between pairs of spheres by means of a mean-field approximation. The resulting fluid–fluid binodal is in fair agreement with that from the free-volume theory, equivalent to the result of the binary mixture DFT. The effective one-component treatment also predicts complete wetting. However, there is also a partial wetting regime, at high ρ_*^r, followed by a sequence of five layering transitions and then a transition to the completely wet state as ρ_*^r is reduced following the gas branch of the binodal. The pattern of surface phase transitions (see figure 5 of [24]) is very similar to that seen in figures 9 and 12 for the AO model, i.e. the first layering transition is quite extended in ρ_*^r and the layering critical point, near $\rho_*^r = 20$, is well removed from the binodal. Subsequent transition lines are reduced in extent and lie close to the binodal. Thus, it is tempting to argue that this effective one-component treatment of the adsorbed sphere–needle mixture mimics what we found for the AO model. But there we argued that it was the incorporation of effective many-body interactions between the colloids that was responsible for the rich layering behaviour; our effective one-component treatment did not yield layering transitions in the case of the AO model. A full understanding of the results for the sphere–needle model is yet to emerge. The precise location of the triple point is important. Indeed a preliminary simulation study of the bulk system [73], using the same effective sphere–sphere potential as in [24], finds that $\rho_{*,\mathrm{crit}}^r \approx 17.5$ and $\rho_{*,t}^r \approx 22.7$, i.e. gas–liquid coexistence is stable over a rather narrow region of ρ_*^r. More significantly, the triple point lies below the onset of the first layering transition found in [24], suggesting that the layering could be occurring in a region where the gas–liquid transition is metastable with respect to gas–solid. This is not the case in the AO model where in both the DFT calculations of

section 4.2 and in the simulation studies of section 4.3, the onset of layering occurs well below the triple point.

A further study [74] was devoted to developing a geometry-based DFT for a ternary mixture of hard-sphere colloids, ideal polymer spheres and vanishingly thin hard needles. The model combines those of AO and of Bolhuis–Frenkel. Both the mutually non-interacting polymers and mutually non-interacting needles act as depletion agents so that rich fluid phase separation can arise. As usual, colloid–colloid, colloid–polymer and colloid–needle interactions are hard. Schmidt and Denton [74] consider two cases: (i) the polymer–needle interaction $\phi_{PN}(r)$ vanishes for all distances r and (ii) it is hard, i.e. $\phi_{PN} = \infty$ if polymer and needle overlap, and zero otherwise. Constructing the DFT for the second case requires a generalization to needles of an earlier DFT treatment [75] of the Widom–Rowlinson model [66] since in the absence of colloids the polymer–needle mixture is of the Widom–Rowlinson type: interactions between like species vanish while unlike particles interact via hard-core repulsion. For case (i), two-phase coexistence between colloid-rich and colloid-poor fluid phases is found. For case (ii), there is the possibility of de-mixing between the polymers and the needles. Moreover, there can be a competition between the depleting effects of (interacting) polymers and needles; the two species compete to generate the attraction between the colloid spheres. Striking demixing fluid phase behaviour is found, with various critical points and a three-phase coexistence region [74]. It would be of considerable interest to investigate structural correlations in the various bulk fluid phases and to consider inhomogeneous situations, such as fluid–fluid or wall–fluid interfaces, in this model system.

A very different kind of confinement from that considered so far is present for fluids adsorbed in porous media. Rather than the well-defined geometries which occur at a planar wall or at fluid–fluid interfaces, irregular and random confinement acts on the adsorbed fluid. In order to model porous media one introduces the so-called quenched–annealed fluid, where the quenched components represent the porous medium in terms of immobilized fluid configurations. Since the quenched components act as an external potential on the annealed (equilibrated) components constituting the adsorbate, the one-body density distribution of the latter can be obtained using standard DFT methods. However, such an approach is computationally demanding since the spatial distribution of the adsorbate is extremely complicated. An alternative approach, termed quenched–annealed DFT, was proposed recently. This treats the quenched components on the level of their one-body density distributions [76]. The minimization condition differs from that of equilibrium (fully annealed) mixtures, as the quenched components are treated as fixed input quantities in the grand potential functional. For the AO model adsorbed in different types of matrices the results of this DFT approach were compared to those from liquid integral equation theory (replica OZ using the optimized random-phase approximation) for the corresponding effective one-component model, where the polymers are integrated out and only the pairwise contributions to the effective Hamiltonian of section 2.1 are taken into account [77]. Thus, the effective interaction between colloids is given by $\phi_{AO}^{eff}(R)$ while the colloid and matrix particles interact via either a hard-sphere potential or $\phi_{AO}^{eff}(R)$. Both approaches predict, consistently, capillary condensation or evaporation, depending on the nature of the matrix–polymer interaction. If a matrix particle excludes both colloid and polymer, condensation occurs, whereas if the matrix excludes only colloid (there is vanishing matrix–polymer interaction) capillary evaporation occurs. The latter refers to the situation where phase separation occurs in the fluid adsorbed in the matrix at chemical potentials for which the reservoir would remain in a single, colloid-rich, liquid phase. The bulk pair correlation functions from DFT are in good agreement with computer simulation results [77]. A very recent study is devoted to demixing and the planar fluid–fluid interface of the AO mixture adsorbed in a matrix of homogeneously distributed hard-sphere particles [78]. Two cases are considered: (i) colloid-sized matrix particles at low packing fractions and (ii) large matrix particles at high packing fractions. The two cases exhibit very different behaviour; for details see [78].

7. Discussion

We have outlined two strategies for tackling the statistical mechanics of *inhomogeneous* colloid–polymer mixtures described by the simplest model that captures the effects of depletion attraction, namely the Asakura–Oosawa–Vrij (AO) model. The first of these, based on the well-trodden 'integrating out' route of McMillan–Mayer theory, is most useful for highly asymmetric mixtures with small size ratio $q < 0.1547$, where there are no three- or higher-body contributions to the effective one-component Hamiltonian for the colloids. The second employs a geometry-based DFT for the mixture that treats the two species on equal footing. Since there is no explicit integrating out of the polymer degrees of freedom, depletion effects are generated internally by the geometrical structure of the functional. This DFT approach has the advantage that it applies to arbitrary size ratios, including those where many-body contributions are known to be important. The main results of our investigations of interfacial properties are presented in sections 3 and 4 where we describe the

density profiles and surface tensions for the free fluid–fluid interface and the properties of the AO mixture adsorbed at a hard wall calculated using the functional derived in [16, 17]. For the free interface we find oscillatory structure in the density profiles on the colloid-rich (liquid) side of the interface for state points where the coexisting liquid density lies on the oscillatory side of the Fisher–Widom line and surface tensions which are in reasonable agreement with experiment. We find that for a highly asymmetric mixture, $q = 0.1$, at state points away from any phase boundary, the AO functional gives a good account of the simulation data for density profiles at a hard wall. For larger size ratios, where fluid–fluid coexistence occurs, the DFT predicts very rich interfacial phase diagrams which display both a wetting transition and several novel layering transitions. The interfacial phase diagram was determined for size ratios $q = 0.6, 0.7$ and 1.0 and we find the topology changes significantly with q. We make a comparison with recent Monte Carlo simulation results for the interfacial phase diagram for size ratio $q = 1$.

Here we discuss further some features of our results. The oscillations we observe in the free interface colloid density profiles are dramatic. They appear to have an amplitude larger than oscillations which have been calculated for simple liquids at state points near the triple point. We argue in section 3 that despite the very low interfacial tension of the colloid–polymer system, the capillary wave fluctuation erosion of the oscillations should not be greater than for a simple liquid. This suggests that colloid–polymer mixtures might provide an excellent opportunity to investigate oscillatory structure at fluid–fluid interfaces, as the large size of colloidal particles makes them well suited to ellipsometric measurements [39, 79]. Oscillations at a free fluid–fluid interface arise when that interface is 'stiff', i.e. for high values of the appropriate reduced surface tension γ^*, and when the density difference between the two coexisting bulk phases is large. Under these conditions the free interface (treated at mean-field level) behaves as a 'wall' and layered structure can develop due to packing effects. These effects are most pronounced near the triple point where both the reduced surface tension and the density difference are largest. Considering the phase diagram for $q = 0.6$, shown in figure 2, and identifying η_p^r with T^{-1}, it is clear that the separation between the critical and triple points is much larger in the present case than for a simple fluid such as argon. It is primarily for this reason that we can obtain such pronounced oscillations in the colloidal density profiles for states near the triple point. By contrast, as the temperature is reduced in simple liquids the oscillations can only grow slightly before the liquid–vapour coexistence region runs out and the triple point, i.e. the crystalline phase, intervenes. One could argue that oscillatory liquid–gas interfaces would be a common feature in simple fluids at sufficiently low temperatures were it not for the onset of crystallization. The AO model can generate oscillations of even larger amplitude than those shown in figure 3. As the size ratio is increased the separation in η_p^r between the critical and triple points grows, e.g. for $q = 1$, $\eta_{p,t}^r/\eta_{p,crit}^r \sim 8$, see figure 18, and γ^* can become rather large—see figure 3. A similar scenario arises for binary mixtures of repulsive Gaussian core particles. There liquid–liquid coexistence can occur over a very large range of total density, since there is no crystalline phase present, and the resulting interfaces can be very 'stiff' leading to predictions of very weak erosion of the oscillations: the exponent in equation (20) is calculated to be about -0.1 [41]. Pronounced oscillatory structure is also well known in the study of liquid metals where there is a large separation between the triple and critical points and the reduced liquid–gas surface tensions are very large. Simulations of the liquid–gas interface of alkali metals [80] and of Ga [81] and X-ray reflectivity experiments on both Ga [82] and Hg [83, 84] all indicate stratification of the ion-density profile, with a spacing of about one atomic diameter, on the liquid side of the interface.

The recent Monte Carlo studies of Chacón and co-workers [43, 44] are significant in this context. These authors constructed classical pair potential (no explicit treatment of the electrons) models of a metal so that the melting temperature T_m was deliberately suppressed relative to the critical temperature T_c, typically $T_m/T_c \lesssim 0.2$. At low temperatures they find high surface tensions and thus a 'stiff' interface which seems to be the origin of the strongly stratified density profiles which they observe. Chacón and co-workers [44] also make the important point that for models of the type they consider, strong stratification can occur over a few atomic layers in the interface even when the bulk liquid is on the monotonic side of the FW line. However, we know the ultimate asymptotic decay into bulk of the density profile must be governed by the behaviour of the bulk pair correlation functions. At very low temperatures $T \sim T_m$, they estimate the erosion of the oscillations to be weak, with the exponent in equation (20) about -0.4. The calculated exponent increases with T to a value of about -1, near the FW line. Monte Carlo results for the density profiles calculated for increasing interfacial area are consistent with the power-law prediction of equation (20) [44]. There are, of course, important differences between the liquid metal models, where the large ratio T_c/T_m arises from the inclusion, albeit empirically, of electronic effects into the pair potential, and the AO model, where the large value of $\eta_{p,t}^r/\eta_{p,crit}^r$ arises from the presence of effective many-

body interactions between the colloids—recall that the latter are responsible for separating the triple and critical points at large size ratios—see the discussion of figure 18.

We turn now to the layering transitions we find in section 4.2. These are a very specific prediction of the AO functional and since they are found in simulation, appear to be a genuine feature of the AO model, rather than an artefact of the DFT.

Although the pattern of the layering transitions observed for $q = 1$ in the simulations of [19] is not identical to that from DFT, the shapes of the density profiles near the transitions are very close to those found in the theory so the layering *phenomena* are certainly the same. We argued in section 4.3 that the occurrence of such transitions, far from $\eta_{p,t}^{r}$, requires the effective many-body interactions that are incorporated into the DFT and into the simulations. Without these contributions the triple and critical points lie much closer together and there is less scope for the layering (and wetting) transitions to manifest themselves at the (stable) gas–hard wall interface. We emphasize, once again, that simulations employing only the effective pair potential $\phi^{\text{eff}}(R; z_p)$ yield a very narrow range, in η_p^r, of stable liquid–gas coexistence. The form of the wall-induced effective interactions must also be important for the occurrence of layering transitions. The effective pair interaction between colloids $\phi^{\text{eff}}(\mathbf{R}_i; \mathbf{R}_j; z_p)$ is a complicated function of the coordinates $\mathbf{R}_i$ and $\mathbf{R}_j$ when the colloids are close to the wall [11]; the strength of the attraction is lowered compared with that of $\phi_{AO}^{\text{eff}}(R_{ij}; z_p)$, which pertains to the homogeneous fluid. It is possible that this reduction in pairwise attraction, caused by the wall reducing the overlap volume of the depletion zones around each colloid, competes with the attractive one-body potential $\phi_{AO}^{\text{wall}}(z; z_p)$ and that this situation favours layering [19, 25]. However, it is fair to say that we do not, as yet, have a full understanding of what gives rise to these curious transitions†. The issues are compounded by the fact that layering transitions were found in an effective one-component DFT calculation for the analogous case of the sphere–needle mixture [24]. Although in this case, see section 6, there remain questions as to how well the one-component theory accounts for the extent of stable liquid–gas coexistence.

Whether the layering transitions remain in models which treat the wall and/or the polymer more realistically remains to be seen. It would be of considerable interest to investigate adsorption at a hard wall for the simple model described in section 5. Incorporating polymer–polymer interactions is expected to reduce substantially the separation between $\eta_{p,t}^{r}$ and $\eta_{p,\text{crit}}^{r}$ (this is also what is found in the simulation studies for SAW models of the polymer [15]) which might make it difficult to observe any layering transitions and indeed the pronounced oscillations found in the colloid density profiles at the free interface for the AO model. Direct simulation studies for colloids and interacting polymers near a wall would be valuable, but extremely demanding! It seems unlikely that such layering transitions could be observed in adsorption experiments as the transition lines lie so close to the bulk coexistence curve that remarkable experimental accuracy would be required to resolve these. Moreover, polydispersity in both colloid and polymer sizes, roughness of the substrate etc. would tend to eliminate what are probably rather subtle and specific features of the AO mixture adsorbed at a hard wall.

We conclude this discussion of layering transitions by returning to the difference between the type of transitions found in the AO model and those found in DFT [51] and in simulation [87] studies of the adsorption of simple gases at strongly attractive substrates. In the latter case the transitions always occur close to the triple point where the density profiles are more highly structured than those shown in section 4.2, i.e. the individual layers are much sharper. When a transition occurs (at fixed T, increasing μ) the jump in the Gibbs adsorption corresponds to the addition of (roughly) one dense 'liquid' layer. As the sequence of transitions progresses the magnitude of the jump in adsorption increases, reflecting the broadening of the outer peaks in the profile and the fact that the local density in one or two of the previous layers also increases at the transition. There can be a very large number of transitions—nine or ten could be discerned in DFT calculations [51]—but their critical points all lie quite close to the triple point T_t. Indeed, within a mean-field treatment the number of transitions can be infinite, i.e. complete wetting of the gas–substrate interface by liquid, which is expected to occur for all $T > T_t$ for strongly attractive substrates, can occur by an infinite sequence of layering transitions out of coexistence. When capillary wave fluctuations in the wetting film are included the number of transitions must be finite, since the liquid–gas interface is always rough (in the statistical mechanics sense). By contrast, for the AO mixture

†It is well known that wetting transitions can depend sensitively on the details of the wall-fluid interactions. For example, in a Landau treatment which includes a surface term of third order in the surface magnetization m_1, which is of opposite sign to the usual linear $-h_1 m_1$ term, Indekeu [85] found a *single* thin–thick transition, followed by a continuous wetting transition on increasing T along the bulk coexistence curve. An equivalent scenario was found by Piasecki and Hauge [86] in a simple DFT treatment of a Yukawa fluid adsorbed at a wall exerting both an attractive exponential and a square-well wall-fluid potential.

adsorbed at a hard wall the onset of layering transitions occurs far below $\eta^{r}_{p,t}$ where the density profiles of the colloid are not as highly structured (see figure 8) and the jump in the adsorption, Γ_c, does not necessarily increase as the sequence increases (but note that the results in section 4.2 refer to a path following the bulk coexistence curve rather than following paths at fixed η^{r}_{p}, equivalent to fixed T.) It is feasible, nevertheless, that within our DFT treatment of the AO mixture there could be an infinite sequence of layering transitions leading to complete wetting of the 'gas'–hard wall interface. Our numerical results do not rule out this scenario. Given that the layering transition lines get shorter and shorter as this sequence progresses it is difficult to ascertain the precise sequence. If this is the correct interpretation, then, as observed, we would not expect to find a substantial pre-wetting line emerging from the wetting point. The simulation results [19] cannot shed much light on this issue; there one expects a finite but large number of transitions before the onset of complete wetting if the attractive one-body wall–fluid potential $\phi^{wall}_{AO}(z; z_p)$ is driving the wetting transition. Note that layering transitions at temperatures above the bulk triple point have been found recently in Gibbs ensemble Monte Carlo simulations of TIP4P water in cylindrical pores [88].

We complete this discussion of layering transitions between distinct adsorbed fluid phases by pointing out that there is much experimental evidence for such interfacial behaviour in *molecular* fluids adsorbed on a graphite substrate under near triple point conditions—see references in [51]. Ellipsometric studies of various liquids adsorbed on Pyrex glass [89] and on mica [90] at low temperatures also provide evidence for layering, i.e. steps in the adsorption isotherms. Steps in the relative adsorption of 2.5-dimethylpyridine in the liquid mixture with water, in contact with solid silica have also been identified as layering transitions [91]. Bonn *et al*. [92, 93] have argued on the basis of ellipsometric measurements, that a series of first-order layering transitions occurs at a *fluid* substrate, i.e. at the liquid–gas interface in a binary methanol–cyclohexane mixture at high temperatures.

The wetting transition in colloid–polymer mixtures is a much more promising candidate for experimental investigation and the basic phenomenon of wetting of a 'hard' substrate by the colloid-rich phase should, in principle, be experimentally observable. Although experiments with colloidal particles have an advantage over those using rare gases or fluids composed of small molecules in that they can be performed at room temperature, issues such as polydispersity obviously complicate matters. Nevertheless, systematic measurements of the contact angle for the liquid–gas meniscus of phase-separated colloid–polymer mixtures, at various compositions and size ratios, in contact with glass walls would be most interesting. Indeed, there are already indications, from contact angle measurements [94, 95], of a transition from partial to complete wetting for a mixture of silica particles and PDMS, with size ratio ~ 0.93, in a solvent of cyclohexane at a glass substrate coated with the same organophilic material as the silica particles (on which PDMS does not adsorb). The transition appears to take place further from the critical point, measured in terms of $\eta^{l}_{c} - \eta^{g}_{c}$, the difference in colloid packing fractions of the liquid and gas, than is found in simulations or in DFT for the AO model—see section 4. Measuring the contact angle for these systems is *not* straightforward, however. Although the static interfacial profile (shape of the meniscus) can be measured using an optical microscope and the capillary length extracted, thereby yielding the liquid–gas surface tension γ, the contact angle depends very sensitively on the precise location of the wall and studies by the Utrecht group [96] were unable to ascertain whether or not a wetting transition occurred for a silica–PDMS mixture. The values of γ which they obtained were close to those measured by the independent spinning drop technique [36, 79], given in figure 3. More recent results from confocal scanning laser microscopy demonstrate the presence of a thick colloidal liquid layer at the glass wall, consistent with complete wetting [63].

As mentioned in section 6, it should also be possible to design experiments which investigate, quantitatively, capillary condensation in simple confining geometries. Such experiments are difficult to perform for atomic fluids but for colloidal systems, where the particle sizes, and hence the confining length scales, are much larger, this is feasible and there are already some observations of the phenomenon in a colloid–polymer mixture [63]. One might also envisage studying some of the more subtle capillary phenomena, such as those associated with interfacial transitions in wedge geometry [97, 98].

Turning now to small size ratios, where the only equilibrium phase transition is the fluid–solid transition, we would encourage further theoretical and simulation studies of adsorption at a hard wall. As mentioned in section 4.1, we did not [11] make any effort to approach closely the fluid–solid phase boundary so we could not address the important issue of how crystalline layers develop prior to bulk crystallization. Various scenarios are possible [11], but given that the wall–colloid depletion potential $\phi^{wall}_{AO}(z; z_p)$ is strongly attractive, for say $q = 0.1$, this might favour an infinite sequence of (crystalline) layering transitions, culminating in complete wetting of the hard wall–fluid interface by a nearly close-packed crystal. However, it is not known how close to the phase boundary the bulk (reservoir) fluid must be before the first adsorbed layer becomes

crystalline. Of course, understanding wall-induced crystallization is not an easy problem. For pure hard spheres at a planar hard wall it is not fully established whether or not there is complete wetting by hard-sphere crystal—although recent simulation studies [73, 99] suggest that this is the case. The nature of the wetting behaviour has important repercussions for heterogeneous nucleation of the crystal [99].

In sections 5 and 6 we considered several extensions of the basic AO model that were designed to incorporate additional physical features pertaining to a real colloid–polymer mixture or to introduce entirely new ingredients, such as orientational degrees of freedom in the case of the sphere–needle mixture. All of these extensions make use of geometry-based DFT; indeed they were constructed with this purpose. Just how accurate the DFT proves to be for the various models remains to be seen for the most part. Where the DFT has been tested in detail for an inhomogeneous situation, it performs very well [71]. We envisage many applications of these extensions to various types of inhomogeneity.

We began this article by praising the virtues of simple models so it is appropriate to ask what other physical problems might be tackled within the context of the basic AO model. In particular, are there situations where depletion attraction is expected to play an important role and where our DFT might prove effective? Recall once more that entropic depletion effects are generated internally—unlike the case of DFT for simple fluids where van der Waals attraction is treated explicitly, usually in a perturbative or mean-field fashion [31]—in our geometry-based approach the attraction between colloids, or between a colloid and a hard wall, arises solely from the geometrical structure of the functional. The solvation of a single (big) hard sphere in a binary AO mixture is of particular interest. Since the planar hard wall can be wet completely by the colloid-rich liquid phase it follows that a liquid film will develop around a big hard sphere immersed in a colloid-poor gas that is very close to bulk coexistence. This circumstance leads to pronounced effects in the solvation free energy or excess chemical potential, measured as a function of the radius of the big sphere, R_b, and of the packing fraction of colloid, say. Indeed the situation mimics that of a simple *liquid* (solvent) adsorbed at a big solvophobic particle (hard sphere), except there drying always occurs, so that a film of gas develops on the sphere when the solvent is close to coexistence [100]. A new feature arising in the AO case is the presence of the layering and the wetting transitions. For sufficiently large R_b, these transitions are still present at the sphere, albeit rounded by finite-size effects, and lead to very striking features in the adsorption, density profiles at contact with the sphere and in the solvation free energy of the sphere [101]. A single hard sphere in the AO mixture serves as an excellent model for investigating subtle effects of curvature on interfacial properties, especially when complete wetting occurs.

One can easily construct the DFT for a ternary mixture consisting of (big) hard spheres, colloidal hard spheres plus mutually non-interacting polymer spheres, i.e. a solution of big hard spheres in the AO solvent. For such a mixture one can determine the solvent-mediated potential between two big spheres or between a big sphere and a wall using a general DFT particle insertion approach [102]. Since the solvent exhibits fluid–fluid phase separation one can investigate the effects of layering, wetting and solvent criticality on the solvent-mediated potentials [101]. In order to implement the DFT particle insertion procedure one requires a density functional that can describe reliably a mixture of the solvent and the big particles in the limit of vanishing density of the big particles [102]. Such functionals are hard to come by (perturbative approaches are generally not appropriate) but the geometry-based DFT for this particular ternary mixture fits the bill†.

Finally we should mention briefly some of the topics that we have *not* covered in this article. There is a rapidly expanding body of work on glass transitions in colloid–polymer mixtures. Strong evidence is emerging for two types of glass; one is repulsion dominated (as in pure hard spheres) and the other is attraction dominated (as occurs when the addition of polymers gives rise to very deep depletion potentials). For an 'Edinburgh model mixture', i.e. PMMA and PS with $q = 0.08$, adding a little polymer (PS) to the hard-sphere colloidal glass, at fixed $\eta_c \sim 0.6$, disrupts the caging structure and brings about crystallization. Adding more polymer results in non-crystallization, there appears to be a re-entrant glass transition [13]. Simulations and mode coupling theory, based on an effective one-component depletion potential, have been used to investigate this behaviour [104, 105]. We have not considered in any detail the situation where $q \gg 1$, i.e. the so-called 'protein limit', where small particles such as proteins or micelles replace the colloids. There is much interesting physics in this limit but it is quite different from the depletion-driven phenomena we have described in this article. Interested readers should consult the recent articles [14, 106, 107] to obtain some overview of this regime. During the course of completing our paper

†Solvent-mediated potentials in the presence of wetting have also been investigated for big Gaussian core particles immersed in a binary mixture of smaller Gaussian particles using the mixture generalization of the mean-field functional (40). See [103].

we were alerted to the work of Forsman *et al.* [108] who extended a DFT developed for polymer solutions to the situation where solvent and monomer particles have different diameters. These authors consider capillary-induced phase transitions when the confining planar surfaces are hard.

The Urbana group [109] have investigated phase diagrams and osmotic compressibilities for silica particles and polystyrene in decalin comparing their results with the PRISM integral equation theory developed by Fuchs and Schweizer [14] and with the free-volume theory of [4]. These authors argue that PRISM accounts for all experimental trends whereas the free-volume approach appears to miss certain aspects of the experimental behaviour, even for theta solvent conditions. Chen *et al.* [110] also present a critique of the AO model for treating real colloid–polymer mixtures. We were also made aware of the work of Paricaud *et al.* [111] who consider bulk fluid–fluid phase separation in a model in which the polymer–polymer and polymer–colloid excluded volume interactions are treated at the same level of the monomeric segments making up the polymer chain, using the Wertheim thermodynamic perturbation theory. Once again we direct interested readers to these papers.

Much of the work described in this article would not have come to fruition without the substantial input of our co-workers, A. R. Denton, A. Esztermann, A. Fortini, M. Fuchs, I. O. Götze, G. Kahl, J. Köfinger, R. Roth, E. Schöll-Paschinger and P. P. F. Wessels. H. Löwen was instrumental in bringing the Bristol and Düsseldorf groups together and provided much stimulus for the research. We are grateful to our experimental colleagues in Utrecht, D. G. A. L. Aarts, E. H. A. de Hoog and, especially, H. N. W. Lekkerkerker, who shared with us their love and knowledge of real colloid–polymer mixtures (and free-volume theory!†). We thank R. Roth for many inspiring discussions about depletion forces, barmaids and nurses and for valuable comments on the manuscript. P. G. Bolhuis, J.-P. Hansen and A. A. Louis kept us busy with a steady supply of pre-prints; we admire their industry and regret that we cannot do more justice to their work in the present article. R. van Roij provided much illuminating insight into matters of integrating out and constructing effective Hamiltonians. We would not have embarked upon the research described here were it not for Marjolein Dijkstra. She introduced us to the subject, explained why it was interesting, carried out the key simulation studies and motivated many of the DFT studies. Marjolein also provided healthy criticism of most of the results. She must share some of the responsibility for the length of this article! The early stages of this research were supported by the British–German ARC Programme (Project 104b) and by EPSRC. RE is grateful to S. Dietrich and his colleagues for their kind hospitality and to the Alexander von Humboldt Foundation for their support under GRO/1072637 during his stay at the MPI in Stuttgart. He also wishes to thank the editors of *Molecular Physics* for their patience in waiting for the article to be delivered.

†There is a special t-shirt describing the virtues of this theory available at a small cost from the Van't Hoff laboratory.

References

[1] Pusey, P. N., 1991, *Liquids, Freezing and Glass Transition*, edited by J. P. Hansen, D. Levesque and J. Zinn-Justin (Amsterdam: Elsevier Science), Chap. 10.
[2] Rutgers, M. A., Dunsmuir, J. H., Xue, J. H., Russel, W. B., and Chaikin, P. M., 1996, *Phys. Rev.* B, **53,** 5043.
[3] Meijer, E. J., and Frenkel, D., 1994, *J. chem. Phys.*, **100,** 6873.
[4] Lekkerkerker, H. N. W., Poon, W. C. K., Pusey, P. N., Stroobants, A., and Warren, P. B., 1992, *Europhys. Lett.*, **20,** 559.
[5] Ilett, S. M., Orrock, A., Poon, W. C. K., and Pusey, P. N., 1995, *Phys. Rev.* E, **51,** 1344.
[6] Asakura, S., and Oosawa, F., 1954, *J. chem. Phys.*, **22,** 1255.
[7] Asakura, S., and Oosawa, F., 1958, *J. Polym. Sci.*, **33,** 183.
[8] Vrij, A., 1976, *Pure appl. Chem.*, **48,** 471.
[9] Gast, A. P., Hall, C. K., and Russell, W. B., 1983, *J. Coll. Int. Sci.*, **96,** 251.
[10] Dijkstra, M., Brader, J. M., and Evans, R., 1999, *J. Phys.: condens. Matter*, **11,** 10079.
[11] Brader, J. M., Dijkstra, M., and Evans, R., 2001, *Phys. Rev.* E, **63,** 041405.
[12] Leal Calderon, F., Bibette, J., and Biasis, J., 1993, *Europhys. Lett.*, **23,** 653.
[13] Poon, W. C. K., 2002, *J. Phys.: condens. Matter*, **14,** R859.
[14] Fuchs, M., and Schweizer, K. S., 2002, *J. Phys.: condens. Matter*, **14,** R239.
[15] Bolhuis, P. G., Louis, A. A., and Hansen, J. P., 2002, *Phys. Rev. Lett.*, **89,** 128302.
[16] Schmidt, M., Löwen, H., Brader, J. M., and Evans, R., 2000, *Phys. Rev. Lett.*, **85**, 1934.
[17] Schmidt, M., Löwen, H., Brader, J. M., and Evans, R., 2002, *J. Phys.: condens. Matter*, **14,** 9353.
[18] Rosenfeld, Y., 1989, *Phys. Rev. Lett.*, **63,** 980.
[19] Dijkstra, M., and van Roij, R., 2002, *Phys. Rev. Lett.*, **89,** 208303.
[20] Schmidt, M., Denton, A. R., and Brader, J. M., 2003, *J. chem. Phys.*, **118,** 1541.
[21] See the review of Likos, C. N., 2001, *Phys. Rep.*, **348,** 267.
[22] Schmidt, M., 2001, *Phys. Rev.* E, **63,** 050201(R).
[23] Brader, J. M., Esztermann, A., and Schmidt, M., 2002, *Phys. Rev.* E, **66,** 031401.
[24] Roth, R., Brader, J. M., and Schmidt, M., 2003, *Europhys. Lett.*, **63,** 549.
[25] Brader, J. M., 2001, PhD Thesis, University of Bristol, Bristol, UK.

[26] Evans, R., Brader, J. M., Roth, R., Dijkstra, M., Schmidt, M., and Löwen, H., 2001, *Phil. Trans. Roy. Soc.* (London) A, **359,** 961.
[27] McMillan, W. G., and Mayer, J. E., 1945, *J. chem. Phys.*, **13,** 276.
[28] Dijkstra, M., van Roij, R., and Evans, R., 1999, *Phys. Rev.* E, **59,** 5744.
[29] Dijkstra, M., van Roij, R., and Evans, R., 2000, *J. chem. Phys.*, **113,** 4799.
[30] Brader, J. M., and Evans, R., 2002, *Physica A*, **306,** 287.
[31] See for example Evans, R., 1992, *Fundamentals of Inhomogeneous Fluids*, edited by D. Henderson (New York: Dekker), Chap. 3, p. 85.
[32] Fisher, M. E., and Widom, B., 1969, *J. chem. Phys.*, **50,** 3756.
[33] Evans, R., Henderson, J. R., Hoyle, D. C., Parry, A. O., and Sabeur, Z. A., 1993, *Molec. Phys.*, **80,** 755.
[34] Evans, R., Leote de Carvalho, R. J. F., Henderson, J. R., and Hoyle, D. C., 1994, *J. chem. Phys.*, **100,** 591.
[35] Dijkstra, M., and Evans, R., 2000, *J. chem. Phys.*, **112,** 1449.
[36] de Hoog, E. H. A., and Lekkerkerker, H. N. W., 1999, *J. phys. Chem.* B, **103,** 5274.
[37] Vliegenthart, G. A., and Lekkerkerker, H. N. W., 1997, *Prog. colloid polym. Sci.*, **105,** 27.
[38] Brader, J. M., and Evans, R., 2000, *Europhys. Lett.*, **49,** 678.
[39] de Hoog, E. H. A., Lekkerkerker, H. N. W., Schulz, J., and Findenegg, G. H., 1999, *J. phys. Chem.* B, **103,** 10657.
[40] Toxvaerd, S., and Stecki, J., 1995, *J. chem. Phys.*, **102,** 7163.
[41] Archer, A. J., and Evans, R., 2001, *Phys. Rev.* E, **64,** 041501.
[42] Mikheev, L. V., and Chernov, A. A., 1987, *Sov. Phys. JETP*, **65,** 971.
[43] Chacón, E., Reinaldo-Falagán, M., Velasco, E., and Tarazona, P., 2001, *Phys. Rev. Lett.*, **87,** 166101.
[44] Tarazona, P., Chacón, E., Reinaldo-Falagán, M., and Velasco, E., 2002, *J. chem. Phys.*, **117,** 3941.
[45] Vrij, A., 1997, *Physica* A, **235,** 120.
[46] Brader, J. M., Evans, R., Schmidt, M., and Löwen, H., 2002, *J. Phys.: condens. Matter*, **14,** L1.
[47] Chen, B., Payandeh, B., and Robert, M., 2000, *Phys. Rev.* E, **62,** 2369.
[48] Archer, A. J., and Evans, R., 2002, *J. Phys.: condens. Matter*, **14,** 1131.
[49] See for example Schick, M., 1990, Liquids at Interfaces, edited by J. Charvolin, J. F. Joanny and J. Zinn-Justin (Amsterdam: North-Holland), chap. 9, p. 415.
[50] Henderson, J. R., 1994, *Phys. Rev.* E, **50,** 4836.
[51] Ball, P. C., and Evans, R., 1988, *J. chem. Phys.*, **89,** 4412.
[52] Louis, A. A., Bolhuis, P. G., Hansen, J. P., and Meijer, E. J., 2000, *Phys. Rev. Lett.*, **85,** 2522.
[53] Warren, P. B., Ilett, S. M., and Poon, W. C. K., 1995, *Phys. Rev.* E, **52,** 5205.
[54] Rosenfeld, Y., Schmidt, M., Löwen, H., and Tarazona, P., 1997, *Phys. Rev.* E, **55,** 4245.
[55] Tarazona, P., and Rosenfeld, Y., 1997, *Phys. Rev.* E, **55,** R4873.
[56] Schmidt, M., 1999, *J. Phys.: condens. Matter*, **11,** 10163.
[57] Tarazona, P., 2000, *Phys. Rev. Lett.*, **84,** 694.
[58] Louis, A. A., Bolhuis, P. G., and Hansen, J. P., 2000, *Phys. Rev.* E, **62,** 7961.
[59] Schmidt, M., 2003, *J. Phys.: condens. Matter*, **15,** S101.
[60] Evans, R., 1990, *J. Phys.: condens. Matter*, **2,** 8989.
[61] Schmidt, M., Fortini, A., and Dijkstra, M., 2003, *J. Phys.: condens. Matter*, **15,** S3411.
[62] Evans, R., and Marini Bettolo Marconi, U., 1987, *J. chem. Phys.*, **86,** 7138.
[63] Aarts, D. G. A. L., and Lekkerkerker, H. N. W., private communication (unpublished), Utrecht University.
[64] Götze, I. O., Brader, J. M., Schmidt, M., and Löwen, H., 2003, *Molec. Phys.*, **101**, 1651.
[65] Schmidt, M., and Denton, A. R., 2002, *Phys. Rev.* E, **65,** 061410.
[66] Widom, B., and Rowlinson, J. S., 1970, *J. chem. Phys.*, **52,** 1670.
[67] Denton, A. R., and Schmidt, M., 2002, *J. Phys.: condens. Matter*, **14,** 12051.
[68] Schmidt, M., and Fuchs, M., 2002, *J. chem. Phys.*, **117,** 6308.
[69] Bolhuis, P., and Frenkel, D., 1994, *J. chem. Phys.*, **101,** 9869.
[70] Barker, J. A., and Henderson, D., 1976, *Rev. mod. Phys.*, **48,** 587.
[71] Bolhuis, P. G., Brader, J. M., and Schmidt, M., 2003, *J. Phys.: condens. Matter*, **15,** S3421.
[72] Roth, R., 2003, *J. Phys.: condens. Matter*, **15,** S277.
[73] Dijkstra, M., private communication (unpublished), Utrecht University.
[74] Schmidt, M., and Denton, A. R., 2002, *Phys. Rev.* E, **65,** 021508.
[75] Schmidt, M., 2001, *Phys. Rev.* E, **63,** 010101(R).
[76] Schmidt, M., 2002, *Phys. Rev.* E, **66,** 041108.
[77] Schmidt, M., Schöll-Paschinger, E., Köfinger, J., and Kahl, G., 2002, *J. Phys.: condens. Matter*, **14,** 12099.
[78] Wessels, P. P. F., Schmidt, M., and Löwen, H., 2003, *Phys. Rev.* E., **68,** 061404.
[79] de Hoog, E. H. A., 2001, Dissertation, Utrecht University, The Netherlands.
[80] Harris, J. G., Gryko, J., and Rice, S. A., 1987, *J. chem. Phys.*, **87,** 3069.
[81] Zhao, M., Chekmarev, D. S., Cai, Z. H., and Rice, S. A., 1999, *Phys. Rev.* E, **56,** 7033.
[82] Regan, M. J., Kawamoto, E. H., Lee, S., Pershan, P. S., Maskil, N., Deutsch, M., Magnussen, O. M., Ocko, B. M., and Berman, L. E., 1995, *Phys. Rev. Lett.*, **75,** 2498.
[83] Magnussen, O. M., Ocko, B. M., Regan, M. J., Penanen, K., Pershan, P. S., and Deutsch, M., 1995, *Phys. Rev. Lett.*, **74,** 4444.
[84] DiMasi, E., Tostmann, H., Ocko, B. M., Pershan, P. S., and Deutsch, M., 1998, *Phys. Rev.* B, **58,** R13419.
[85] Indekeu, J. O., 1989, *Europhys. Lett.*, **10,** 165.
[86] Piasecki, J., and Hauge, E. H., 1987, *Physica A*, **143,** 87.
[87] Fan, Y., and Monson, P. A., 1993, *J. chem. Phys.*, **99,** 6897.
[88] Brovchenko, I., Geiger, A., and Oleinikova, A., 2001, *Phys. Chem. chem. Phys.*, **3,** 1567.
[89] Law, B. M., 1990, *J. Colloid Interface Sci.*, **134,** 1.
[90] Beaglehole, D., and Christenson, H. K., 1992, *J. phys. Chem.*, **96,** 3395.
[91] Sellami, H., Hamraoui, A., Privat, M., and Olier, R., 1998, *Langmuir*, **14,** 2402.
[92] Bonn, D., Wegdam, G. H., Kellay, H., and Nieuwenhuizen, T. M., 1992, *Europhys. Lett.*, **20,** 235.

[93] Bonn, D., Kellay, H., and Wegdam, G. H., 1993, *J. chem. Phys.*, **99,** 7115.
[94] Wijting, W. K., Besseling, N. A. M., and Cohen Stuart, M. A., 2003, *Phys. Rev. Lett.*, **90,** 196101.
[95] Wijting, W. K., Besseling, N. A. M., and Cohen Stuart, M. A., 2003, *J. phys. Chem.* B, **107,** 10565.
[96] Aarts, D. G. A. L., van der Wiel, J. H., and Lekkerkerker, H. N. W., 2003, *J. Phys.: condens. Matter*, **15,** S245.
[97] Rascón, C., and Parry, A. O., 2000, *Nature* (London), **407,** 986.
[98] Bruschi, L., Carlin, A., and Mistura, G., 2002, *Phys. Rev. Lett.*, **89,** 166101.
[99] Auer, S., and Frenkel, D., 2003, *Phys. Rev. Lett.*, **91,** 015703.
[100] Evans, R., Roth, R., and Bryk, P., 2003, *Europhys. Lett.*, **62,** 5360.
[101] Roth, R., and Evans, R., unpublished.
[102] Roth, R., Evans, R., and Dietrich, S., 2000, *Phys. Rev.* E, **62,** 5360.
[103] Archer, A. J., and Evans, R., 2003, *J. chem. Phys.*, **118,** 9726.
[104] Pham, K. N., Puertas, A. M., Bergenholtz, J., Egelhaaf, S. U., Moussaid, A., Pusey, P. N., Schofield, A. B., Cates, M. E., Fuchs, M., and Poon, W. C. K., 2002, *Science*, **296,** 104, and references therein.
[105] Dawson, K., Foffi, G., Fuchs, M., Götze, W., Sciortino, F., Sperl, M., Tartaglia, P., Voigtmann, T., and Zaccarelli, E., 2001, *Phys. Rev.* E, **63,** 011401.
[106] Sear, R., 2001, *Phys. Rev. Lett.*, **86,** 4696.
[107] Bolhuis, P. G., Meijer, E. J., and Louis, A. A., 2003, *Phys. Rev. Lett.*, **90,** 068304.
[108] Forsman, J., Woodward, C. E., and Freasier, B. C., 2002, *J. chem. Phys.*, **117,** 1915.
[109] Shah, S. A., Chen, Y. L., Schweizer, K. S., and Zukoski, C. F., 2003, *J. chem. Phys.*, **118**, 3350.
[110] Chen, Y. L., Schweizer, K. S., and Fuchs, M., 2003, *J. chem. Phys.*, **118,** 3880.
[111] Paricaud, P., Varga, S., and Jackson, G., 2003, *J. chem. Phys.*, **118,** 8525.